Arabian Journal of Chemistry (2023) **16**, 104711

King Saud University

Arabian Journal of Chemistry

www.ksu.edu.sa
www.sciencedirect.com

ORIGINAL ARTICLE

Performance evaluation and assessment of the corrosion inhibition mechanism of carbon steel in HCl medium by a new hydrazone compound: Insights from experimental, DFT and first-principles DFT simulations

M. En-Nylly [a], S. Skal [b], Y. El aoufir [c], H. Lgaz [d,*], Raihana J. Adnin [e], Awad A. Alrashdi [f], A. Bellaouchou [b], M.R. Al-Hadeethi [g], O. Benali [a], T. Guedira [a], H-S. Lee [h,*], S. Kaya [i], S.M. Ibrahim [j]

[a] *Laboratory of Organic Chemistry, Catalysis, and Environment, Faculty of Science, Ibn Tofail University, B.P 133, 1400 Kenitra, Morocco*
[b] *Laboratoire des Matériaux Nanotechnologie et Environnement, Université Mohamed V Agdal. Faculté des Sciences, Av. Ibn Battouta, BP 1014 Rabat. Morocco*
[c] *Laboratory of Organic Chemistry, Catalysis, and Environment, Faculty of Science, Ibn Tofail University, B.P 133, 1400 Kenitra, Morocco*
[d] *Innovative Durable Building and Infrastructure Research Center, Center for Creative Convergence Education, Hanyang University ERICA, 55 Hanyangdaehak-ro, Sangnok-gu, Ansan-si, Gyeonggi-do 15588, Republic of Korea*
[e] *Department of Smart City Engineering, Hanyang University-ERICA, 55 Hanyangdaehak-ro, Sangnok-gu, Ansan-si, Gyeonggi-do 15588, Republic of Korea*
[f] *Chemistry Department, Umm Al-Qura University, Al-Qunfudah University College, Saudi Arabia*
[g] *Department of Chemistry, College of Education, University of Kirkuk, Kirkuk 36001, Iraq*
[h] *Department of Architectural Engineering, Hanyang University-ERICA, 55 Hanyangdaehak-ro, Sangnok-gu, Ansan-si, Gyeonggi-do 15588, Republic of Korea*
[i] *Sivas Cumhuriyet University, Health Services Vocational School, Department of Pharmacy, 58140 Sivas, Turkey*
[j] *Department of Biochemistry, College of Science, King Saud University, P.O. Box 2455, Riyadh 11451, Saudi Arabia*

Received 10 January 2023; accepted 20 February 2023
Available online 27 February 2023

* Corresponding authors.
E-mail addresses: hlgaz@hanyang.ac.kr (H. Lgaz), ercleehs@hanyang.ac.kr (H-S. Lee).
Peer review under responsibility of King Saud University.

Production and hosting by Elsevier

https://doi.org/10.1016/j.arabjc.2023.104711

KEYWORDS

Corrosion inhibitor;
Hydrazone;
Carbon steel;
Density Functional Theory;
Molecular dynamics;
XRD

Abstract In the present work, a new hydrazone compound, namely N'-[(Z)-(4-chlorophenyl)methy lidene]-2-(5-methoxy-2-methyl-1H-indol-3-yl)acetohydrazide, noted HTH, was selected to protect carbon steel against corrosion in 1.0 mol/L HCl. Different chemical, electrochemical, and surface characterization techniques such as scanning electron microscope coupled with X-ray energy dispersion (SEM/EDX) were used to investigate the corrosion inhibition performance. Electrochemical data showed that the effectiveness of the inhibitor improved with increasing concentration, reaching 98% at the optimal concentration of 10^{-3} mol/L. The results of potentiodynamic polarization measurements showed that hydrazone acted as a mixed-type inhibitor. The EIS results showed an increase in polarization resistance accompanied by a noticeable decrease in $C_{eff,dl}$ values. In the temperature range of 303 K-333 K, hydrazone protected carbon steel by 89%, showing high resistance to temperature effect. The analysis of the steel surface by SEM/EDX confirmed that the effectiveness of the hydrazone was attributed to the formation of a protective layer on the surface of the metal. Quantum chemical calculations revealed insights into the chemical reactivity of the tested hydrazone while first-principles density functional theory (DFT) and molecular dynamics (MD) simulation supported the experimental conclusions and showed outstanding adsorption ability of HTH on the Fe(1 1 0) surface. First-principles DFT simulations showed that the HTH molecule was more stable in a parallel adsorption mode.

1. Introduction

Highly concentrated commercial hydrochloric acid has become an important chemical reagent used in many applications (Chaouiki et al., 2020b). It destroys scales in pipes, removes traces of cement on tiles, is also used to remove unwanted scales and rust in metal finishing industries, acidification of oil wells in oil recovery, etc.(Lgaz et al., 2020a). It can also be used as a remover for metals that have been corroded, so it is one of the causes of metals decomposing either by chemical or electrochemical reactions. The industrial world already has widespread consumption of iron and its alloys, especially carbon steel, due to its physical and chemical properties and its low manufacturing cost (Chafiq et al., 2020b).

The interaction between metal and acid causes corrosion by chemical and electrochemical reactions. This phenomenon leads to the loss of the main characteristics of iron, such as hardness or resistance (Salghi et al., 2017). Corrosion occurs as a result of cross-sectional losses, having lower ductility, ultimate resistance, and yield strength. It decreases the life of structures, resulting in structural vulnerability and leading to a structural failure (Lgaz et al., 2020b). Many solutions and efforts have been demonstrated to reduce the corrosion process, including the use of corrosion inhibitors which are one of the most effective and low-cost strategies (Oyekunle et al., 2019).

The use of inhibitors at low concentrations reduces or prevents the interaction of steel with its environment and thus reduces the rate of corrosion (Chafiq et al., 2020b). It is now well established from differ-

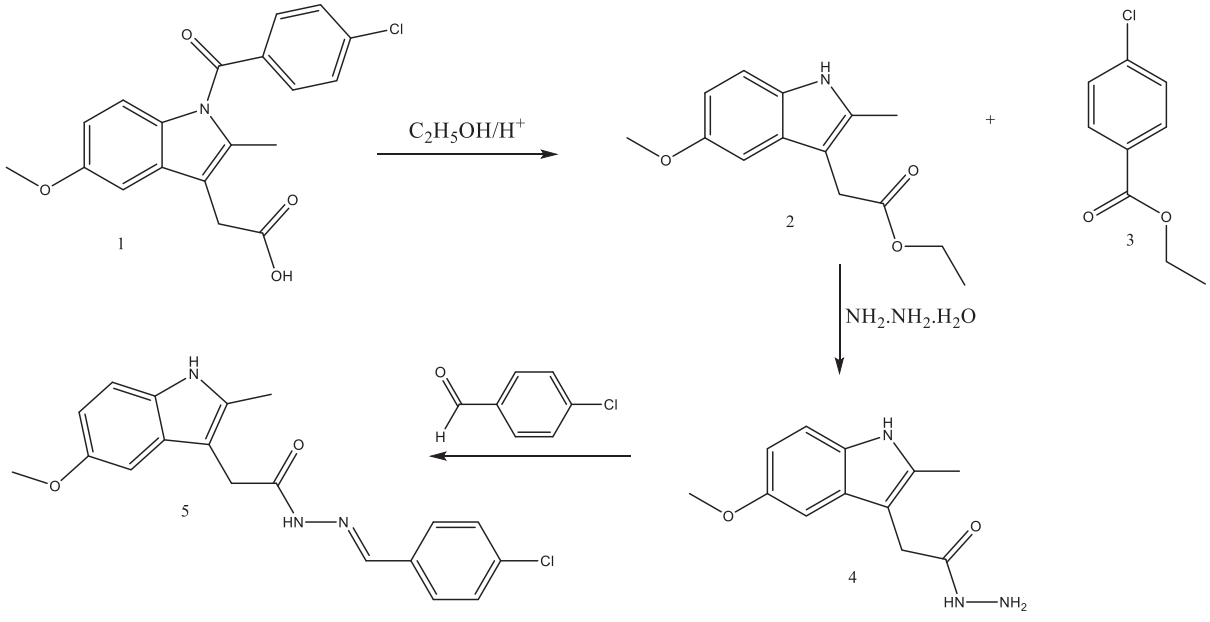

Scheme 1 Synthesis procedure for (5) (= HTH) compound.

ent studies that organic compounds containing heteroatoms such as N, S, P, and O, functional groups, bonds, and aromatic heterocyclic rings play a vital role in the inhibition and attenuation of corrosion in acidic environments (Fadhil et al., 2019). These inhibitors are absorbed on the surface of carbon steel, forming a protective layer that prevents increased corrosion rates. Among the most widely used organic corrosion inhibitors, the hydrazone class of organic compounds is one of the most effective ones. Hydrazones are a class of organic compounds with the structure $R_1R_2C = N - NR_3R_4$, having outstanding structural and electronic properties (Vargas et al., 2021).

These prominent compounds have been widely used in the bioconjugation and functionalization of polymers, due to the ease of introducing these functions into biomolecules and probes. Hydrazones have exerted a dominant influence in many other research areas as well (Vargas et al., 2021). The 5-methoxy-2-methyl-3-indoleacetic acid (MMIAA) is one of the impurities found in the NSAID Indomethacin (IND) drug, and therefore a lot of efforts have been made to identify and separate this unwanted chemical (Riasová et al., 2018). The MMIAA compound can be valorized through the conversion of its free carboxylic group into hydrazone derivatives. This synthetic approach can also suppress the gastrointestinal toxicity side effect of most NSAIDs (Mohamed et al., 2015; Tammara et al., 1994). Many studies (Shanbhag et al., 2008) have shown that hydrazone has positive effects on steel in a hydrochloric acid medium. According to the results of these studies, hydrazone is one of the most effective inhibitors in that it significantly reduces the corrosion rate of steel (Chafiq et al., 2021; Khamaysa et al., 2021). The effectiveness of hydrazone varied from study to study due to the difference in type and nature of the used hydrazone. The value of efficiency is not less than 60%, and often not more than 95%.

On the other hand, it has been proved that the corrosion inhibition process is a complex phenomenon that cannot be easily understood from only experimental studies. In this context, great efforts have been made to implement computational methods to investigate the adsorption characteristics of organic compounds on metal surfaces. Quantum chemical calculations are one of the classical methods to study the electronic and structural properties of organic compounds, aiming to provide a better explanation of their corrosion inhibition characteristics (Dehghani et al., 2019; Gece, 2008; Zaher et al., 2022). Besides, molecular dynamics simulation made it possible to simulate the adsorption and interaction of organic compounds on metal surfaces in the presence of a simulated solution (Ebenso et al., 2021; Shahmoradi et al., 2022). However, these two approaches are very limited in describing the bond formation and breaking upon adsorption, which is an essential criterion for simulating the corrosion inhibition process by organic compounds. To overcome this limit, other methods such as first-principles density functional theory (DFT) and self-consistent-charge density-functional tight-binding method (SCC-DFTB) are needed to get more realistic insights into the corrosion inhibition process (Guo et al., 2017; Lgaz and Lee, 2022).

This work reports the corrosion inhibition behaviour of carbon steel in a hydrochloric acid solution without and with different concentrations of a newly synthesized hydrazone compound, namely N'-[(Z)-(4-chlorophenyl)methylidene]-2-(5-methoxy-2-methyl-1H-indol-3-yl)acetohydrazide (HTH). Its effectiveness in different concentrations and temperatures was evaluated using electrochemical and gravimetric tests. Moreover, the uninhibited and inhibited surface of samples was characterized by scanning electron microscopy coupled with energy dispersive X-ray (SEM/EDX). Besides, computational studies using density functional theory (DFT), first-principles DFT, and molecular dynamics (MD) simulation were carried out to investigate the inhibitor's electronic and adsorption features and its adsorption configuration on Fe(1 1 0) surface.

2. Materials and methods

2.1. Synthesis of the inhibitor

The title compound *N*'-[(*Z*)-(4-chlorophenyl)methylidene]-2-(5-methoxy-2-methyl-1*H*-indol-3-yl)acetohydrazide (5) was prepared according to the following procedures and Scheme 1:

2.1.1. Synthesis of ethyl (5-methoxy-2-methyl-1H-indol-3-yl) acetate (2)

Access of absolute ethanol was added to 0.01 mol of indomethacin in the presence of 5 mL conc. H_2SO_4. The mixture was refluxed for 7 h. The mixture was poured into crushed ice and neutralized with $NaHCO_3$. The ester was separated as an oily layer, then washed with water three times and extracted with diethyl ether 2 × 50 mL and then recrystallized from cyclohexan to afford the title compound as silver crystals with m.p = 74–76 °C.

IR(KBR): (C═O ester 1710), (NH3316), (C—H aliphatic 2832–2975), (═C—H aromatic 3002) cm^{-1}.

2.1.2. Synthesis of 2-(5-methoxy-2-methyl-1H-indol-3-yl) acetohydrazide (4)

To a solution of 0.01 mol from compound (2) in ethanol, 0.06 mol of hydrazine hydrate was added and the mixture was refluxed for 24 h. The reaction mixture was cooled and the precipitate was formed, collected, and recrystallized from ethanol to afford the title compound as pale yellow crystals with m.p = 166–168 °C. IR(KBR): (C = O amide 1656), (NH-NH_2 3288–3215), (C—H aliphatic 2835–2971) cm^{-1}.

2.1.3. Synthesis of (5) N'-[(Z)-(4-chlorophenyl)methylidene]-2-(5-methoxy-2-methyl-1H-indol-3-yl)acetohydrazide

An equimolar mixture of compound 4 and 4-chlorobenzaldehyde in absolute ethanol was refluxed with catalytic amounts of glacial acetic acid for 6 h. The mixture was cooled and the precipitate was formed, collected and recrystallized from ethanol to afford the title compound 5 with m.p = 188–190 °C. IR(KBR): (C═O amide 1648), (—CH═N— 1609), (NH 3295), (C—H aliphatic 2851–2922) cm^{-1}.

^{1}H NMR (400 MHz, DMSO): δ = 3.8(s, 3H, OCH_3), 2.3(s, 3H, CH_3), 3.6(s,2H, —CH_2), 10.6(s, 1H, NH), 11.3(s,1H, NH), 8.2(s,1H, —CH═N—), 6.8–7.7 (m, 7H, aromatic protons in two phenyl rings). ^{13}C NMR δ = 13.0(CH_3), 34(—CH_2), 55 (—OCH_3),43 (2C, 103–155(fourteen aromatic carbons in two phenyl rings and pyrrol moiety), 146 (C═N), 173 (C═O amide).

2.2. Materials and chemicals

The metal used as a working electrode in all the experimental tests is carbon steel. Its chemical composition is presented in Table 1.

The HCl solution (1 mol/L) was prepared from a dilution of 86 mL of 37% hydrochloric acid solution (Sigma Aldrich) with distilled water. Before each test or immersion, carbon steel in

Table 1 Chemical composition of carbon steel.

Atom	Fe	C	Si	Mn	S	Cr	Ti	Ni	Co	Cu
Weight (%)	98.388	0.371	0.229	0.681	0.014	0.076	0.012	0.058	0.010	0.161

the solution must be treated to obtain good and reliable results. Firstly, we polish the surface with a rotating disk containing abrasive paper of granulometry rangy 180, 220, 400, 600, and 1200 to treat it well, and then washing it with distilled water and wipe it until it dries up. The used concentration range of the tested inhibitor was selected after pre-trial tests to be from 10^{-6} mol/L to 10^{-3} mol/L.

2.3. Electrochemical measurements

In all electrochemical test experiments, three electrodes immersed in the electrolyte are used. These electrodes form a classical three-electrodes cell that consists of a saturated calomel electrode (SCE) as a reference electrode, the platinum (Pt) electrode served as a counter electrode, and a working electrode (WE) made of carbon steel, leaving an area of 1 cm^2 exposed to the electrolyte. Electrochemical tests were performed using the potentiostat PGZ401 connected to a computer. The electrochemical data were acquired by the electrochemical analysis software 'VoltaMaster 4.0′. Carbon steel was immersed in hydrochloric acid (1 mol/L) for 30 min until the open circuit potential (OCP) was relatively stable.

Electrochemical impedance measurements were performed in a signal amplitude of 10 mV with a frequency range of 100 kHz to 100 Hz. The potentiodynamic polarization measurements were set from −650 to −250 mV/SCE with a scan rate of 1 mv/sec. The data obtained from electrochemical experiments are converted into semicircular curves or Tafel curves using Volta-master and fitted using EC-Lab software.

2.4. Scanning electron microscopy coupled with energy dispersive X-ray spectrometry

Scanning electron microscope JEOLJSM-IT 100 and X-ray energy dispersions were used to perform surface carbon steel testing. The SEM pictures were studied after the carbon steel was immersed for 24 h in 1 mol/L HCL solution with and without inhibitor. The elemental analysis of the layer generated on the surface of the carbon steel was performed using energy-dispersive X-ray spectrometry.

2.5. Computational details

2.5.1. DFT and MD details

The Dmol3 program in Material Studio Software was used to optimize the geometry of the hydrazone molecule according to the generalized gradient approximation (GGA) with the Perdew-Burke-Enzerhof (PBE) functional (Weston et al., 2012). The Conductor-like Screening Model (COSMO) was used to simulate the effect of water as a solvent during the calculations (Heidari et al., 2021). Full details are reported in the supplementary material.

To determine the best adsorption configuration of the hydrazone molecule, a molecular dynamics simulation was carried out using Forcite code implemented in Materials Studio. The unit cell of iron, exported from the database of Material studio software, was cleaved at the surface (1 1 0) and replicated 8 times in the × and y direction. To reduce the effect of periodic replicas, a space of 30 Å was inserted at the z-axis of the created super-cell. After adding 500 water molecules and the optimized hydrazone molecule into the super-cell, the adsorption system was geometrically optimized according to the Smart algorithm (Mehmeti and Podvorica, 2018) using the COMPASSIII force field (Han et al., 2016). MD simulations were carried out under the NVT ensemble (canonical, i.e., the number of particles N, the volume V, and the temperature T of the system were kept constant), room temperature, 1 fs time step, and 1000 ps simulation time. All other MD simulation details were "default" values of Ultra-fine quality of Forcite module.

2.5.2. First-principles DFT simulations

First-principles DFT simulations were carried out within the framework of spin-polarized DFT using the CASTEP code (Kokalj et al., 2021). The exchange–correlation energy was described within the generalized gradient approximation (GGA) parameterized by Perdew-Burke-Ernzerh (PBE) (Perdew et al., 1996). The empirical dispersion correction was used to accurately describe the effect of van der Waals (vdW) interactions (Grimme, 2006). The energy cut-off for the plane-wave basis was set at 30 Ry. All convergence thresholds were default "Fine" quality values in the CASTEP module. Monkhorst–Pack Brillouin zone k-point grids of (8x8x8) and (2x2x1) were used for the optimization calculation of the bulk lattice parameters and adsorption models, respectively. The initial lattice parameter of iron was 2.862 Å while the optimized one is 2.858 Å, confirming that selected methods and models were reasonable.

The surface Fe(1 1 0) was built by constructing a periodic multi-slab model with a (5x5) supercell and a vacuum spacing of 20 Å along the z direction to account for spurious interactions between slabs. The hydrazone molecule was placed on the top side of the slab. The two bottom-most atomic layers were fixed to bulk positions whereas all other degrees of freedom were allowed to relax. A cubic box of 30 Å in size was created for first-principles DFT calculations of standalone molecules. Inkscape software was used for the post-processing of all figures. The total energies of isolated hydrazone (noted E_{mol}), Fe(1 1 0) iron surface (noted E_{surf}), and hydrazone/Fe(1 1 0) adsorption systems (noted $E_{mol/surf}$) were used to determine the interaction energy as:

$$E_{inter} = E_{mol/surf} - \left(E_{mol} + E_{surf}\right) \quad (1)$$

3. Results and discussion

3.1. Potentiodynamic polarization curves

Potentiodynamic polarization curves are one of the essential studies to know and understand the interactions that occur

on the surface of the steel and the mechanism of anodic and cathodic reactions. Therefore, the relationship between the corrosion current density and the corrosion potential can provide a better understanding of these interactions. To carry out this study, the carbon steel was immersed for 30 min in a solution of hydrochloric acid (1 mol/L) in the presence and absence of the inhibitor with different concentrations ranging from 10^{-3} to 10^{-6} mol/L. Fig. 1 shows the potentiodynamic polarization curves of carbon steel in 1 mol/L HCl with and without inhibitor. The data extracted from the polarization diagrams (Tafel), including the corrosion potential (E_{corr}) and the corrosion current density (i_{corr}), as well as the cathodic and anodic Tafel slopes (β_c, β_a) are summarized in Table 2. The table also includes the efficiencies of the inhibitor which are calculated from the corrosion current densities by the following equation (Chafai et al., 2019):

$$\eta_{PDP}(\%) = \frac{i^{\circ}_{corr} - i_{corr}}{i^{\circ}_{corr}} \times 100 \quad (2)$$

where i_{corr} and i°_{corr} represent the corrosion current densities for an inhibited and uninhibited acid solution, respectively.

It can be observed from Fig. 1 that the increase in the inhibitor concentration generates a decrease in cathodic and anodic Tafel slopes (β_c, β_a). The current density corrosion (i_{corr}) decreased to a minimum value of 32 $\mu A/cm^2$ at a concentration of 10^{-3} mol/L for the hydrazone compound, according to the retrieved results. It can be seen from the curves that increasing the concentration of hydrazone inhibitor causes a reduction in cathodic and anodic current density, with a wide range of linearity, showing that Tafel's law has been appropriately validated (Chafiq et al., 2020a). According to previous studies (Fadhil et al., 2019), this behaviour can be explained by the presence of hydrazone inhibitor molecules leading to forming and gathering on the surface of the steel to create a protective layer.

In addition, the displacement of E_{corr} values allows us to classify the molecules as cathodic or anodic. Generally, in the presence or absence of the inhibitor, if the values of E_{corr} are greater than 85 mV/SCE, the inhibitor molecules are classified as cathodic or anodic type (Salghi et al., 2017; Singh et al., 2016). If, however, the E_{corr} values are less than 85 mV/SCE, it is classified as mixed type (cathodic and anodic). In this study, the hydrazone compound is classified as a mixed type as demonstrated in Table 2.

From the obtained results, the inhibitory efficiency reached 94% at the 10^{-3} mol/L concentration, which is the highest value in these conditions. This percentage indicates that the hydrazone compound effectively affects the corrosion process under acidic conditions. Many studies have been carried out on hydrazone but it is always noticed that there is a difference in the percentages of effectiveness, which could be due to the number of donor groups present in the molecular structure of compounds (Lgaz et al., 2019). The inhibitor used in the present study contains two donor groups Cl and OCH_3, electron donor groups by mesomeric effect, which increases the electrical density of the azomethine group (—C═N—). This would affect the adsorption strength which may be higher by sharing electrons of different reactive sites with the metal surface (Lgaz et al., 2019).

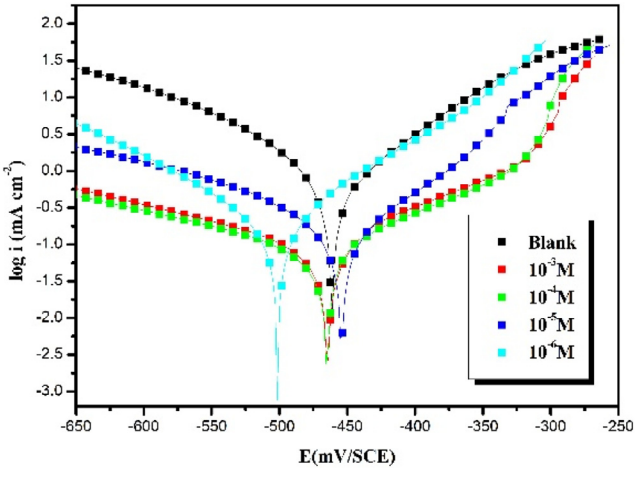

Fig. 1 Potentiodynamic polarization curves of carbon steel in 1.0 mol/L HCl without and with different concentrations of HTH at 303 K.

3.2. Electrochemical impedance spectroscopy measurements

Electrochemical impedance spectroscopy measurements are a robust non-destructive procedure to investigate the mechanism of electrochemical processes of carbon steel immersed in hydrochloric acid. Fig. 2 shows the Nyquist diagrams and the Bode plots obtained for carbon steel in uninhibited and inhibited acidic solutions containing different concentrations of the inhibitor molecule.

The Nyquist impedance plots show that the diameters of the curves increase with an increase in the concentration of inhibitor. This increase is associated with the resistance of the metal. We note that all EIS plots of the inhibitor have non-perfect semicircles. This type of diagram generally indicates that the corrosion reaction is controlled by a charge transfer process. In addition, the reason why the semicircles keep the same shape in the presence and absence of the inhibitor can be explained by the fact that the corrosion mechanism of carbon steel does not change in both cases (Khamaysa et al., 2021). The Bode diagrams show the logarithm of the impedance modulus |Z| and phase angle as a function of the logarithm of the frequency. The impedance modulus |Z| is used as a measure of corrosion protection (Id et al., 2021). It is clear from the results that as the concentration of the inhibitor increases, the modulus of impedance at the lower frequency increases, and the capacitance of the inhibitor is also increased, which means that the carbon steel is better protected against corrosion in the presence of the inhibitor. The increase in phase angle is due to its protective capacity on the surface of carbon steel. This is done by forming an adsorption layer at the metal interface and thus preventing the corrosion inhibitor molecules from penetrating the carbon steel surface (Damej et al., 2022; Nwokolo et al., 2022).

The electrical equivalent circuit shown in Fig. 3 is used to analyze the impedance plots in the presence and absence of the inhibitor. The equivalent circuit consists of an electrolyte resistance (R_S) in series and is connected with a parallel constant phase element (CPE) with polarization resistance (R_p). The CPE was employed instead of pure capacitance because of the carbon steel's heterogeneous surface. The impedance

Table 2 Electrochemical parameters of carbon steel derived after extrapolating the PPCs of inhibited and uninhibited HCl solution at 303 K.

[Inhibitor] (mol/L)	i_{corr} (μA/cm2)	E_{corr} (mV/SCE)	β_c (mV/dec)	β_a (mV/dec)	η_{PDP}(%)
Blank	594	−456	91	80	–
10^{-6}	154	−499	95	80	74
10^{-5}	84	−452	86	70	86
10^{-4}	51	−461	84	180	91
10^{-3}	32	−462	71	72	94

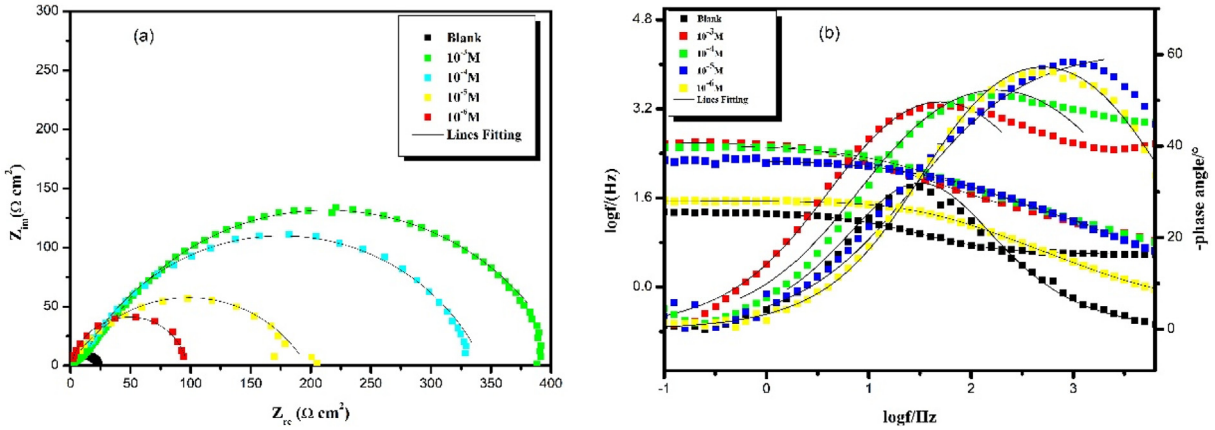

Fig. 2 Electrochemical impedance spectra of carbon steel in 1.0 mol/L HCl without and with different concentrations of HTH at 303 K; (a) Nyquist and (b) Bode plots.

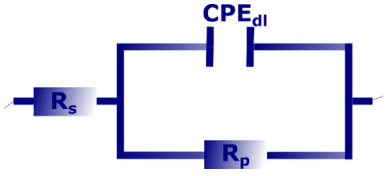

Fig. 3 Electrical equivalent circuit used to fit the impedance data.

of the CPE (Z_{CPE}) is specified by the equations below (Obot et al., 2015; Olasunkanmi et al., 2016):

$$Z_{CPE} = Q^{-1}(i\omega)^{-n} \tag{3}$$

where Q stands for the CPE constant; i = $(-1)^{1/2}$ is the imaginary number; ω is the angular frequency (radious), and the heterogeneity measure is denoted by *n* (Ouakki et al., 2021; Oyekunle et al., 2019).

The effective capacitance of the double layer ($C_{eff\cdot dl}$) is determined using the obtained CPE (Q) parameters by Brug's equations. When the dispersion of the time constant is produced by indigenous inhomogeneities along with the interface, Brug's equation can be utilized to calculate the $C_{eff\cdot dl}$ (Pareek et al., 2019; Perdew et al., 1996).

$$C_{effdl} = Q_{dl}^{1/n}\left[\frac{1}{R_s} + \frac{1}{R_{CT}}\right]^{n-1/n} \tag{4}$$

The performance of the inhibitor is evaluated from EIS tests by calculating the inhibition efficiency as follows (Dutta et al., 2017):

$$\eta_{EIS}(\%) = \left[\frac{R_p^{inh} - R_p^{\circ}}{R_p^{inh}}\right] \times 100 \tag{5}$$

Where R_p° and R_p^{inh} are the polarization resistance without and with the addition of the inhibitor, respectively.

From the results of the impedance spectroscopic analysis presented in Table 3, it can be seen that the addition of hydrazone leads to an increase in R_p while the values of the effective double-layer capacitance (C_{effdl}) decreases. The decrease in the effective double-layer capacitance values is attributed to the decrease in the dielectric constant or double-layer capacitance as the thickness of the formed inhibitor layer increases (Pareek et al., 2019). It is clear that the increase in R_p values is related to the increase in inhibitor concentration; this increase creates a protective barrier against corrosion due to adsorption on the steel surface (Salghi et al., 2017). The table also shows that the 10^{-3} mol/L concentration achieved a 94% efficiency, which is the highest percentage for this inhibitor at 303 K. In most cases and through many studies, the efficiency values of the hydrazone inhibitor vary between 80 and 95%, so it is considered one of the most widely used inhibitors (Chaitra et al., 2016; Singh et al., 2019). It can be concluded from the results obtained that at each increase in R_p with increasing inhibitor concentration, a protective layer is formed, which leads to a decrease in the corrosion process. The inhibitor molecules act by forming this layer on the steel surface, which reduces the charge transfer process. Replacing water molecules, the inhibitor molecules of the hydrazone increase the thickness of the layer to provide better protection for the carbon steel (Lgaz et al., 2020a).

Table 3 Electrochemical impedance spectroscopy (EIS) parameters of carbon steel in the absence and presence of inhibitor concentrations at 303 K.

[Inhibitor] (mol/L)	R_s (Ω cm^2)	n	Q (μF cm^{-2} S$^{(\alpha-1)}$)	R_p (Ω cm^2)	$C_{eff,dl}$ (μF cm^{-2})	η_{PDP}(%)
Blank	1.084	0.8004	873	22.35	151	–
10^{-6}	0.519	0.8240	411	95.63	67	76
10^{-5}	0.690	0.7966	345	196.3	40	88
10^{-4}	3.240	0.7395	244	334.1	19	93
10^{-3}	3.184	0.7426	186	1396.9	14	98

3.3. Temperature effect

The objective of studying the influence of temperature on carbon steel corrosion is to understand the stability of hydrazone molecules at high temperatures. Temperature is a factor responsible for changing the behaviour and reaction of carbon steel in an acid medium. To obtain sufficient information on the effect of temperature, potentiodynamic polarization curves (PDP) and electrochemical impedance spectroscopy measurements were carried out for carbon steel in the 1.0 mol/L HCl medium with and without the inhibitor at its optimal concentration (10^{-3} mol/L) at a temperature range of 303 K-333 K.

3.3.1. Potentiodynamic polarization curves

Tafel curves have been used to understand the effect of temperature on the corrosion reaction of carbon steel in hydrochloric acid with and without inhibitor at an optimum concentration of 10^{-3} mol/L. The experiment was conducted at different temperatures ranging from 303 to 333 K. Fig. 4 summarizes the obtained results.

Fig. 4 shows that the corrosion current density increases as the temperature rises from 303 K to 333 K, both in the presence and absence of the inhibitor. We also see that the cathodic curve is parallel, implying that the H^+ reduction process follows the same activation mechanism. Table 4 summarizes the results of the effect of temperature on carbon steel in the presence and absence of the inhibitor at an optimum concentration of 10^{-3} mol/L.

The table shows that the cathodic and anodic Tafel slopes (β_c, β_a) increase with increasing temperature for both the inhibited and uninhibited systems. Furthermore, the results suggest that when the hydrazone component is present, the values of i_{corr} (253 μA/cm^2) increase slightly with increasing temperatures, as opposed to the acidic medium, which showed a noticeable increase (2250 μA/cm^2). These data indicate that i_{corr} increased slightly in the presence of the hydrazone compound at high temperatures compared to its considerable increase in the acidic medium. The efficiency of hydrazone changes slightly towards low values, reaching 88% at 333 K. However, this performance is very high considering the experimental conditions and other organic corrosion inhibitors, which explain that the inhibitor molecules are stable at high temperatures (Chkirate et al., 2021; Dehri and Özcan, 2006). It can be said that despite the increase in temperature, the inhibitor efficiency decreases slightly due to the strong interaction of π-bonds and lone pair electrons on —NH, —N═N—, and —C═N— groups with the steel surface (Cordero et al., 2008).

3.3.2. Electrochemical impedance spectroscopy measurements

Fig. 5 represents the Nyquist diagrams and modulus of carbon steel in a 1 mol/L HCl solution in the presence of an optimum concentration of 10^{-3} mol/L of the hydrazone at different tem-

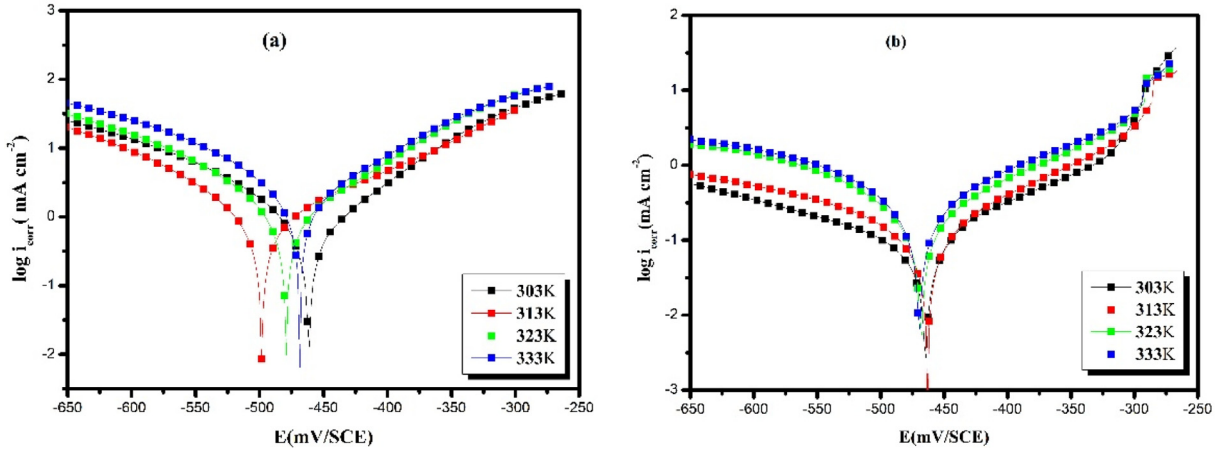

Fig. 4 Potentiodynamic polarization curves of carbon steel in 1.0 mol/L HCl without (a) and with 10^{-3} mol/L of HTH (b) at different temperatures.

Table 4 Electrochemical parameters for carbon steel corrosion in 1 mol/L HCl at different temperatures in the absence and presence of 10^{-3} mol/L HTH.

Medium	T (K)	E_{corr} (mV/SCE)	i_{corr} ($\mu A/cm^2$)	β_c (mV/dec)	β_a (mV/dec)	η_{PDP}(%)
Blank	303	−456	594	91	80	–
	313	−496	804	110	92.5	–
	323	−476	940	88	94.1	–
	333	−466	2250	115	118	–
Blank	303	−462	32	71	72	94
+	313	−460	60	67	108	92
10^{-3} mol/L HTH	323	−464	99	70	68	89
	333	−466	253	148	132	88

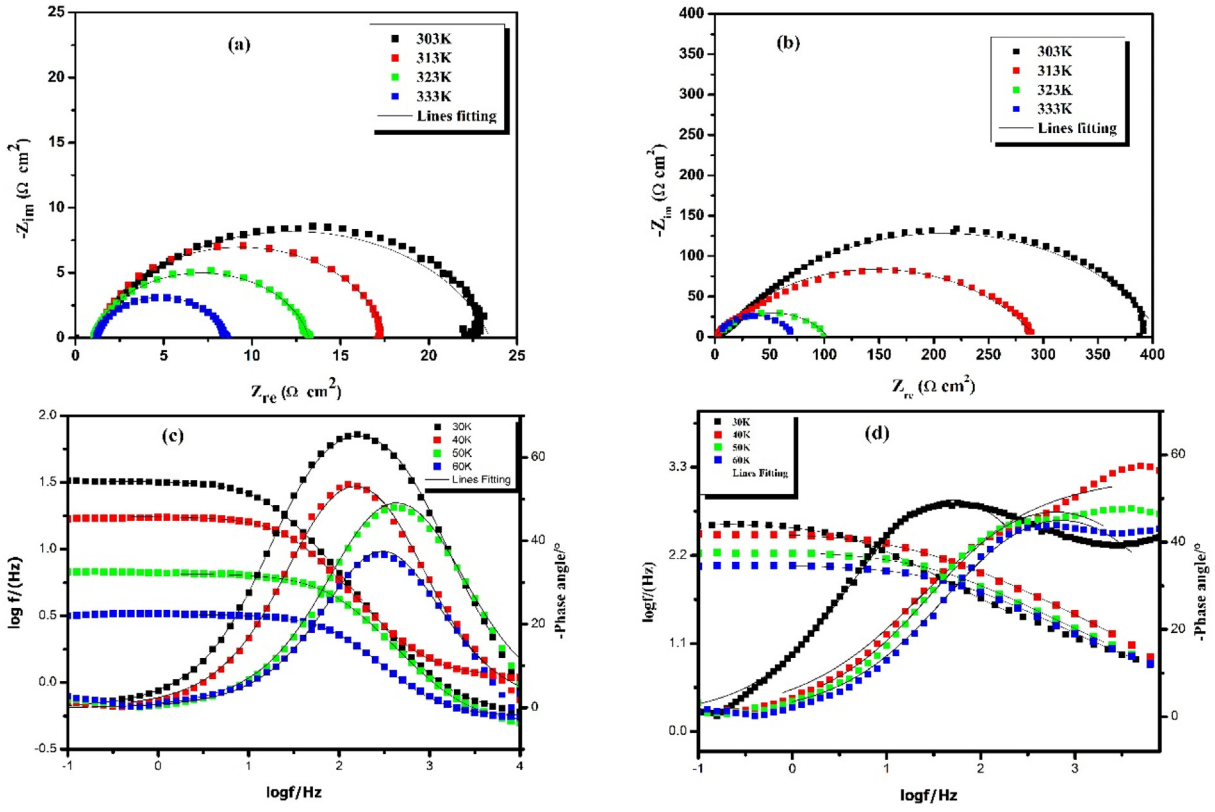

Fig. 5 Electrochemical impedance spectra of carbon steel in 1.0 mol/L HCl without (a, c) and with 10^{-3} mol/L of HTH (b, d) at different temperatures.

peratures ranging from 303 to 333 K. Fig. 5 shows that the diameter of the semicircle reduces as the temperature rises, indicating that the efficacy of the inhibition is influenced by temperature. Table 5 summarizes the results of parameters of carbon steel in inhibited and uninhibited acid solutions derived from EIS measurements at various temperatures ranging from 303 K to 333 K at a concentration of 10^{-3} mol/L for the inhibited solution.

Table 5 shows that as temperature increases, the polarization resistance decreases from 22.35 to 7.3 Ω cm^2 for the uninhibited solution and from 397 to 67 Ω cm^2 for the inhibited solution. At 333 K, the inhibitory efficiency decreases to a maximum value of 89%. It can be seen that the decrease is insignificant at high temperatures. This can be explained by the fact that the inhibitory molecules are stable and strongly adsorbed on the steel surface, forming a robust protective layer. In addition, as the corrosion inhibition process is strongly affected by temperature, it can be concluded that the adsorption of hydrazone molecules at high temperatures is significantly more important than their desorption, mostly because of chemical interactions between active sites of HTH molecules and vacant d-orbitals of iron.

From Bode representation in Fig. 5, it can be seen that the increase in temperature leads to a decrease in the phase angle values and the impedance modulus /Z/. This is consistent with the Nyquist plots and is explained by the fact that some molecules, especially physically interacting with the steel surface would desorb from the steel surface, therefore leading to an increased steel area exposed to the acidic solution.

Table 5 Electrochemical impedance spectroscopy (EIS) parameters for carbon steel corrosion in 1 mol/L HCl at different temperatures in the absence and presence of 10^{-3} mol/L HTH.

Medium	T (K)	R_s (Ω cm^2)	n	Q (μF cm^{-2} S$^{(\alpha-1)}$)	R_p (Ω cm^2)	$C_{eff,\ dl}$ (μF cm^{-2})	η_{PDP}(%)
Blank	303	1.084	0.8004	873	22.35	151	–
	313	1.189	0.900	541	16.35	250	–
	323	1.004	0.897	586	12.17	261	–
	333	1.144	0.896	644	7.3	301	–
Blank	303	3.184	0.742	186	1396.9	14	94
+	313	0.479	0.856	211	292	44	94
10^{-3} mol/L HTH	323	2.071	0.842	354	100	91	87
	333	1.761	0.860	377	67	114	89

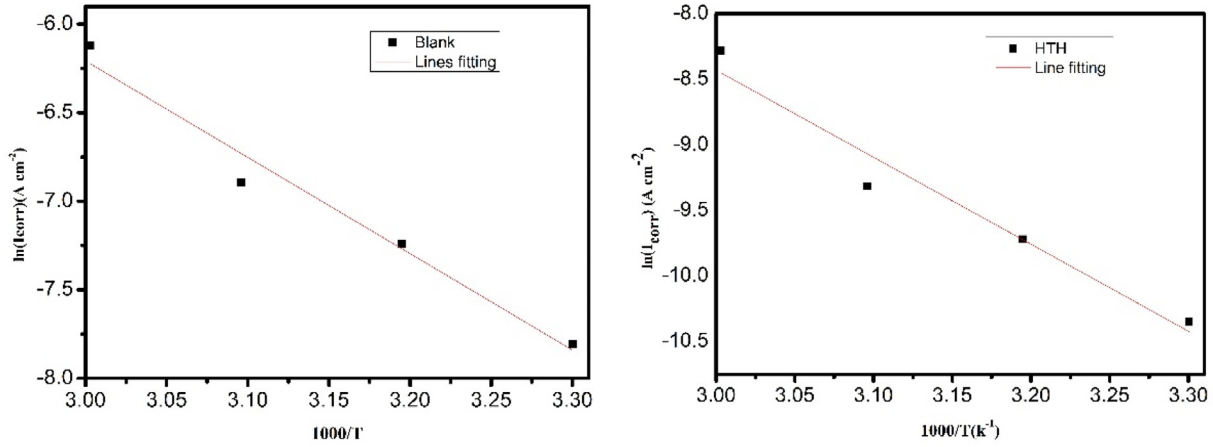

Fig. 6 Arrhenius plots of the corrosion rate for carbon steel in 1.0 mol/L HCl in absence (a) and presence of 10^{-3} mol/L of HTH (b). and (b)AAE.

Chaouiki et al. (Chaouiki et al., 2020b) have confirmed that the hydrazone as (E)-N′-(2,4-dimethoxybenzylidene)-2-(6-met hoxynaphthalen-2-yl),(E)-N'-(4-methoxybenzylidene)-2-(6-met hoxynaphthalen 2-yl)propane hydrazide compound's adsorption on the surface of carbon steel in 1 mol/L HCl solution is stable in the temperature range of 303 K-333 K. They showed that the hydrazone inhibitor still can effectively protect the carbon steel at high temperatures.

The Arrhenius equation was used to analyze the effect of temperature on the corrosion of carbon steel in terms of activation energy. The results of the Tafel extrapolation were used to calculate the standard activation energy E_a. Fig. 6 illustrates Arrhenius diagrams of carbon steel in 1 mol/L HCl solution in the absence and presence of hydrazone at an optimal concentration of 10^{-3} mol/L at temperatures ranging from 303 K to 333 K. The slope of the straight line produced by graphing 1000/T according to ln was used to calculate the value of the activation energy (E_a) according to the Arrhenius formula:

$$i_{corr} = Aexp(-\frac{E_a}{RT}) \quad (6)$$

The carbon steel in inhibited solution has an activation energy value of 55.19 kJ mol^{-1}. The value of the non-inhibited solution is 45.24 kJ mol^{-1}. The inhibitor solution has high activation energy because it produces a protective layer that limits metal dissolution by raising the energy barrier for charge and mass transfer (Chafiq et al., 2020b). Consequently, the process of dissolving the inhibitory system is slow (Chaouiki et al., 2020a).

3.4. Adsorption isotherm models

One of the most common mechanisms of organic inhibitor compounds is adsorption if it is not a criterion to be classified as a corrosion inhibitor (Bockris et al., 1998). It depends on many factors, including the charge and nature of the metal surface, the degree of corrosion reaction, solvent adsorption, and the electronic characteristics of the metal surface (Singh and Singh, 2015). The adsorption isotherm models were used to determine the nature of the adsorption of organic inhibitor molecules on the carbon steel surface (Serhan et al., 2019). Experimentally generated data were correlated to isothermal models to facilitate the comparison of inhibitor compounds. The degree of surface covering (θ) obtained from potentiodynamic polarization measurements at 303 K at varied inhibitor concentrations is fitted to several isotherms such as the Langmuir, Frumkin, and Temkin isotherms. Fig. 7 depicts the linear regression coefficient values of Langmuir, Frumkin, and Temkin isotherms. We conclude that Langmuir represents the best fit for our experimental data. The Langmuir model equation is as follows (Döner et al., 2011):

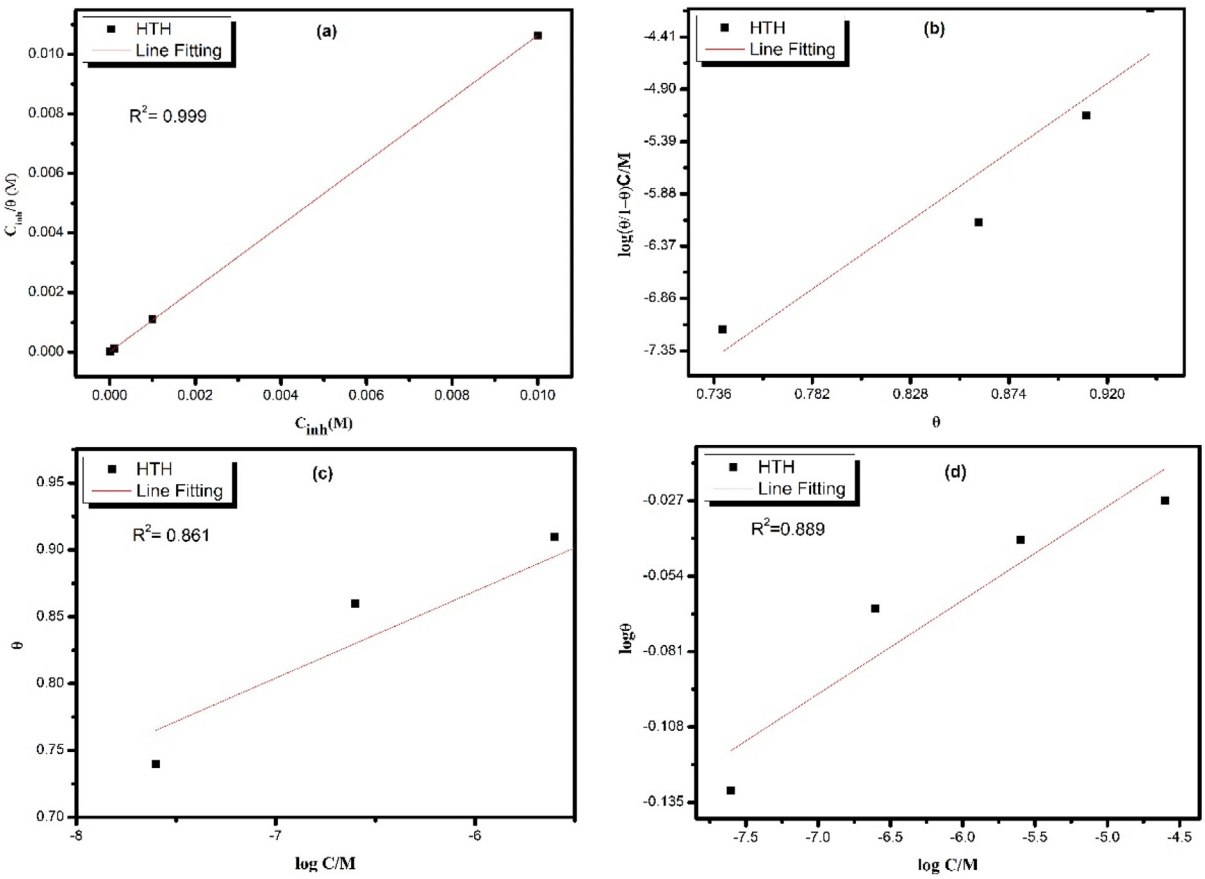

Fig. 7 Adsorption isotherm models for the adsorption of inhibitor molecules on carbon steel in 1.0 mol/L with different concentrations of HTH at 303 K; (a) Langmuir isotherm, (b) Frumkin isotherm, (c) Temkin isotherm, and (d) Freundlich isotherm.

$$\frac{C_{inh}}{\theta} = \frac{1}{K_{ads}} + C \tag{7}$$

Where C_{inh} symbolizes the concentration of hydrazone, and K_{ads} signifies the adsorption equilibrium constant. The value of K_{ads} can be determined from the intercept of the straight line. K_{ads} is also related to the standard free energy of adsorption (ΔG_{ads}) by the following equation (Chaouiki et al., 2020a).

$$K_{ads} = \frac{1}{55.5}\exp\left(-\frac{\Delta G_{ads}}{RT}\right) \tag{8}$$

where 55.5 is the molar concentration of water in the solution expressed in mol L^{-1}, R is the gas constant (8.314 J K^{-1} mol^{-1}) and T is the absolute temperature (K).

The hydrazone inhibitor's K_{ads} (633195.95 L mol^{-1}) value shows that the inhibitor molecules can strongly adsorb on the steel surface. The value of ΔG_{ads} is equal to −43.76 kJ mol^{-1}. Many previously published works use the ΔG_{ads} values to make decisive conclusions about an inhibitor's adsorption on metal surfaces (Dutta et al., 2015; Guo et al., 2020; Tang et al., 2018; Verma et al., 2018); however recent studies indicated that this approach is not always true and should be considered with strict precautions (Kokalj, 2022; Walczak et al., 2019). Therefore, adsorption isotherm data are reported as semi-quantitative descriptors of the isotherm shape and no decisive conclusions about adsorption mechanisms can be made based on this study (Solmaz et al., 2014a; Solmaz et al., 2014a; Tammara et al., 1994).

3.5. Surface morphological study

SEM analysis is one of the most effective ways of examining the surface morphology of corroded and inhibited metals. Carbon steel was immersed in hydrochloric acid solution with and without inhibitor at 303 K to examine its surface morphology. Fig. 8(a-b) shows SEM images of the surface morphologies of the carbon steel immersed in blank and inhibited solution containing 10^{-3} mol/L HTH. There are differences between the two SEM images; image (a) shows that the surface of the steel has been heavily exposed to corrosion in aggressive solutions due to the presence of numerous depressions, pits, and roughness. On the other hand, we can see in image (b) that the percentage of damage has decreased. The surface is smoother in the presence of an ideal concentration of hydrazone inhibitor. The corrosion rate decreases because of the formation of a protective layer by adsorption of the hydrazone molecules.

EDX was used to determine the initial composition of carbon steel samples before and after the addition of the hydrazone inhibitor. From Fig. 8(c) and Table 6, it can be seen that carbon steel contains high percentages of iron, oxygen, and carbon for the uninhibited solution. The spectrum demonstrates that the intensity of the peaks of Fe, Cl, C is high while we notice in the EDX spectrum in the presence of the inhibitor, Fig. 8d and Table 6 that the intensity of the peaks decreases significantly, where the percentage of iron reaches 47.51% instead of 52.49%. The percentage of carbon also decreased

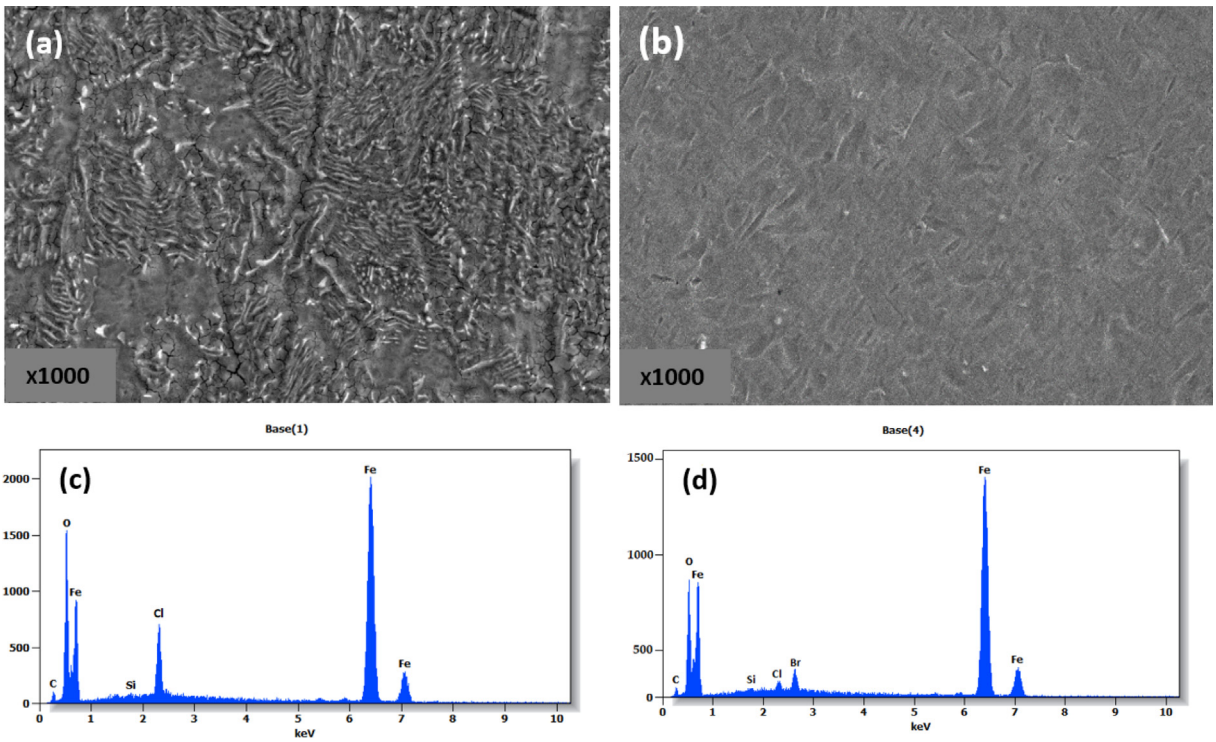

Fig. 8 SEM images of carbon steel immersed for 24 h in blank and HCl solution inhibited with 10^{-3} mol/L of HTH at 303 K.

by 3.75% instead of 6.16%, Cl is 3.66% instead of 6.08%. This decrease indicates that the density of the active corrosion sites has been reduced. This confirms the inhibitor's activity on the carbon steel surface. Furthermore, the presence of the N atom as a result of the introduction of the hydrazone compound demonstrates the existence of inhibitor functional groups on the surface of carbon steel. Inhibitor molecules are adsorbed on the steel surface, forming a protective layer protecting it from corrosion. This is explained by the impact of the aromatic rings and the hydrazide group, which enhances the hydrazone inhibitor's adsorption on the steel surface.

3.6. Computational studies

3.6.1. Quantum chemical calculations

Quantum chemical calculations (QCCs) are one of the most classical ways to assess the reactivity and electronic properties of organic compounds (Islam and Kaya, 2018). In corrosion inhibition studies, QCCs have been applied to investigate the adsorption characteristics and reactivity of corrosion inhibitors (Lgaz et al., 2021). Quantum chemical parameters have been also used to correlate the reactivity of corrosion inhibitors with their quantum chemical parameters; however, it has been shown that this approach has many limitations and cannot be used to make decisive conclusions about an inhibitor's performance (Kokalj et al., 2021). It still can provide useful information about the reactivity of individual molecules such as potential adsorption sites. Herein, quantum chemical parameters are calculated for neutral and protonated HTH molecules to assess its global and local reactivity indices.

Frontier molecular orbitals, i.e., the highest occupied molecular orbital (HOMO) and lowest uncopied molecular orbital (LUMO) and their corresponding energies (E_{HOMO} and E_{LUMO}) are one of the well-known quantum chemical parameters that estimate the electron donating (in case of HOMO) and electron-accepting (in case of LUMO) power of a given molecule (Quadri et al., 2022). A widespread HOMO *iso*-surface on the entire molecule of the inhibitor or a particular part indicates that it can donate and share electrons with accepting chemical species (Olasunkanmi et al., 2016; Zaher et al., 2022). Likewise, a highly distributed LUMO *iso*-surface indicates that the corresponding molecule or part of it can accept electrons from electron-donating species (Olasunkanmi et al., 2016; Zaher et al., 2022). Inspection of Fig. 9, which shows the HOMO and LUMO *iso*-surfaces distributed on the optimized molecular structure of neutral and protonated THT molecules, indicates that 5-methoxyindole part is responsible for electron-donating while the chlorophenyl and hydrazone moieties are the main electron accepting parts.

Table 6 The percentage of atoms for carbon steel in 1.0 mol/L HCl without and with inhibitor was analyzed from EDX spectra.

Element		C	O	Si	Cl	Fe	N
Atom %	Blank	6.16	34.92	0.35	6.08	52.49	–
	Inhibitor	3.75	29.49	0.29	3.66	47.51	15.3

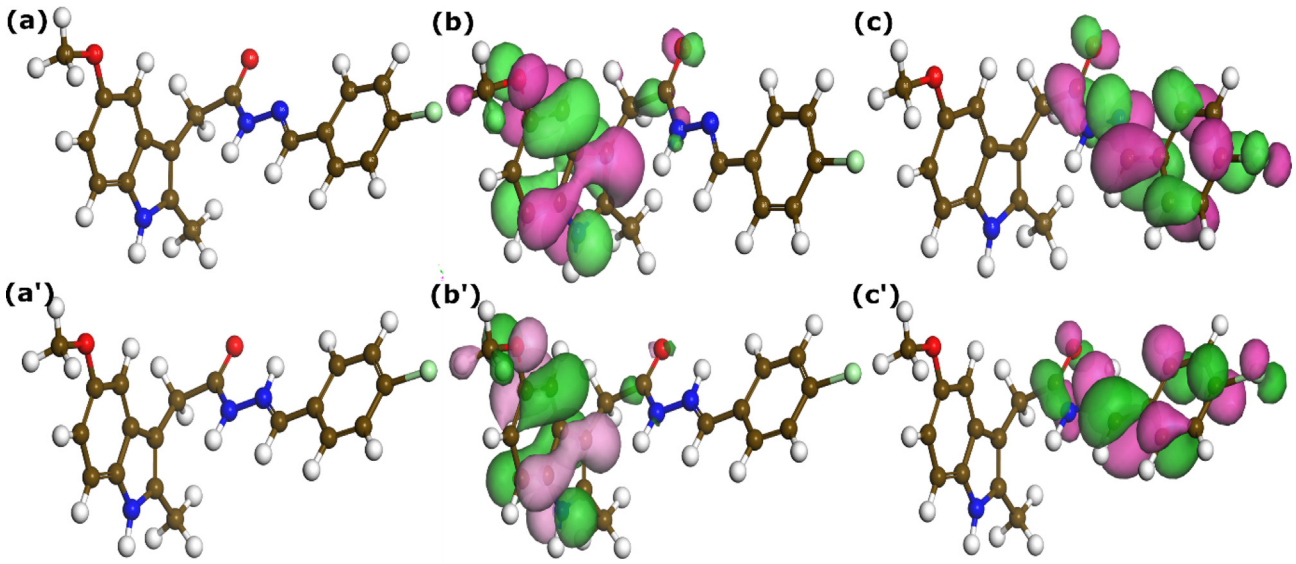

Fig. 9 Optimized molecular structure (a)-(a') and frontier molecular orbital *iso*-surfaces HOMO (b)-(b') and LUMO (c)-(c') of neutral (a)-(c) and protonated (a')-(c') HTH molecules obtained by DFT at GGA/PBE level.

Table 7 Quantum chemical parameters of neutral and protonated HTH molecules calculated after its geometry optimization by DFT at GGA/PBE level.

Compound	E_{HOMO}	E_{LUMO}	ΔE	IE	EA	η	χ	ω	σ	ΔN
Neutral HTH	−5.052	−2.74	2.312	5.052	2.74	1.156	3.896	6.565	0.865	0.399
Protonated HTH	−6.602	−3.749	2.853	6.602	3.749	1.4265	5.1755	9.388	0.701	−0.124

The corresponding HOMO and LUMO energies of neutral and protonated HTH molecules are −5.052 and −2.74 eV, and −6.6.2 and −3.749 eV, respectively (Table 7). It can be noted that the electron-donating ability of the molecule decreased after protonation while its electron-accepting tendency increased, which is a highly expected result. The energy gap, which is defined as the difference between frontier molecular orbital energies is a key factor in investigating a molecule's stability. A molecule with a high energy gap would have high stability and therefore be less reactive when interacting with other chemical species and vice versa (Lgaz et al., 2021). The quantum chemical parameters of HTH are listed in Table 7. From the data in Table 7, it can be seen that the neutral hydrazone has a lower energy gap value compared with the protonated one. It indicates that the neutral form would have more ability to interact with chemical species (Gece, 2008). On the other hand, the fraction of transferred electron (ΔN) of protonated molecule shows a negative value compared to the neutral one, which indicates that the protonated form of the HTH compound cannot participate in electron-donating upon interaction with other chemical species (Saha et al., 2016). Most of the other quantum chemical parameters follow the same trend as they are derived from HOMO and LUMO energies.

Global reactivity descriptors, as their name may imply, give general information about inhibitor's reactivity without specifying the most potential adsorption sites. In contrast, local reactivity indices such as Fukui functions provide more precise information about the ability of each atom in the molecule to

Table 8 The values of Fukui function indices of the HTH molecules calculated using DFT/GGA.

atom	f_k^+	f_k^-
C (1)	0.002	0.064
C (2)	0.001	0.091
C (3)	0.000	0.033
C (4)	0.002	0.042
C (5)	0.003	0.070
C (6)	0.003	0.047
N (7)	0.004	0.076
C (8)	0.004	0.043
C (9)	0.002	0.066
O (10)	0.002	0.077
C (11)	0.001	0.020
C (12)	0.001	0.014
C (13)	0.010	0.013
C (14)	0.046	0.009
N (15)	0.031	0.005
N (16)	0.112	0.005
C (17)	0.110	0.008
C (18)	0.052	0.002
O (19)	0.061	0.028
C (34)	0.064	0.003
C (35)	0.040	0.002
C (36)	0.065	0.003
C (37)	0.046	0.002
C (38)	0.053	0.003
Cl(41)	0.081	0.005

donate or accept electrons to/from interacting species. In other words, a molecule can have only a limited number of atoms or a functional group responsible for its corrosion inhibition performance. Knowing this detailed reactivity of each part of the molecule would be very helpful in designing new corrosion inhibitors with high performance. Table 8 lists the Fukui function indices of the investigated HTH molecule. The Fukui function can be used to identify the sites within the molecule that is available for nucleophilic and electrophilic attacks. Atomic sites, where the Fukui function is large, are softer and vice versa (Obot et al., 2015). The electrophilic Fukui index f_k^+ characterizes the sites for nucleophilic attacks. The nucleophilic Fukui index f_k^- describes preferred sites for attack by electrophiles (Bassey, 2014; Gómez et al., 2006). In Table 8, it is obvious that atoms C(14), N(16), C(17), O(19), C(34), C (36), and Cl(41) exhibit the highest electrophilic Fukui index f_k^+, thus acting as preferred atomic sites to accept electrons during a nucleophilic attack (Pareek et al., 2019). On the other side, atoms C(1), C(2), C(5), N(7), C(9), and O(10) have the highest nucleophilic Fukui index f_k^-, suggesting that they are favorable sites for donating an electron to accepting species (Pareek et al., 2019). These results strengthen the previous conclusions from experimental tests that the molecule under investigation has several reactive atomic sites available for accepting and sharing electrons with vacant d-orbitals of iron, thus providing high protection against acid corrosion.

3.6.2. Molecular dynamics simulation

Classical molecular dynamics simulation has emerged as an excellent theoretical tool in corrosion inhibition research (Obot et al., 2018). In recent years, molecular dynamics simulation has become very popular in corrosion inhibition studies to investigate the adsorption configurations of inhibitor molecules on metal surfaces in the presence of a simulated corrosive solution. Even though in most MD studies of corrosion inhibition only classical forcefields are used to model the interaction between inhibitor molecules and metal surfaces, which cannot provide insights into the bond formation and breaking upon adsorption (Kokalj, 2021), it is still very useful in understanding the adsorption behavior of inhibitor molecules in presence of other particles such as water molecules and corrosive ions. Herein, MD simulation was performed for one inhibitor molecule interacting with Fe(1 1 0) surface in presence of 1450 water molecules, 10 chlorides, and 10 hydronium ions to mimic the

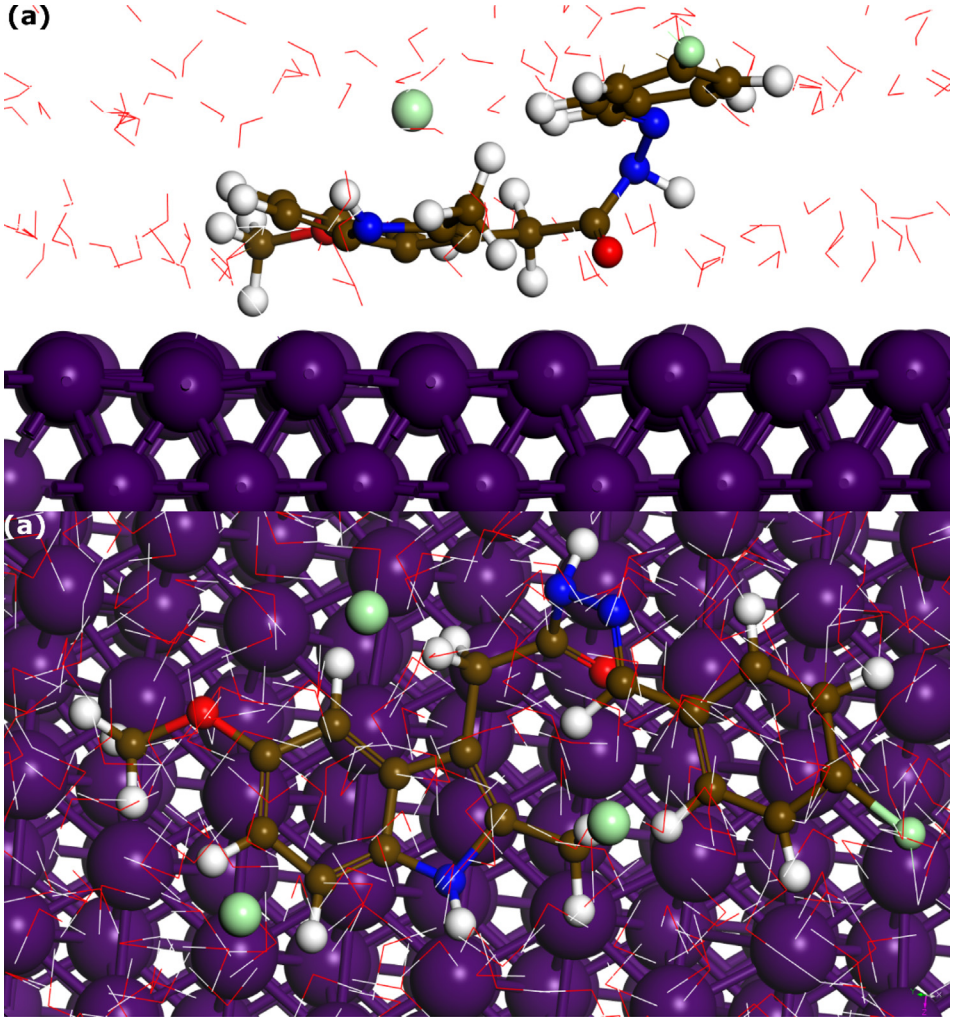

Fig. 10 Snapshots of the optimized adsorption configuration of HTH on Fe(1 1 0) surface by molecular dynamics simulation; (a) Side view and (b) top view.

corrosion inhibition process. Fig. 10 represents the adsorption configuration of HTH on Fe(1 1 0) equilibrated for 5000 ps MD simulation. It can be observed that the 5-methoxyindole of the THT molecule tends to exhibit a parallel disposition over the iron surface, with the carbonyl group also in close contact with iron atoms. Such disposition can maximize the interaction between HTH's adsorption sites and iron atoms. It is well-documented that most large-size organic compounds tend to adopt a parallel adsorption mode when interacting with metal surfaces, forming strong covalent bonds with vacant *d*-orbitals of iron atoms. In presence of water and other particles, it would be very competitive for the HTH to get adsorbed on the Fe(1 1 0) surface. Therefore, it can be concluded from the adsorption configuration that HTH has a strong affinity to iron atoms. At this level, MD simulation is useful and helpful in understanding the adsorption characteristics of inhibitor molecules in presence of other particles, however, it overestimates the interaction energy of adsorbing molecules and thus this parameter is not considered (Kokalj, 2021). A more robust way to determine the interaction energy of HTH on Fe(1 1 0) surface is through the first-principles method.

3.6.3. First-principles DFT simulation

Opposite to quantum chemical calculations and molecular dynamics simulation, first-principles DFT simulation provides very significant physical insights into the adsorption of inhibitor molecules on metal surfaces (Damej et al., 2023). In addition to the most stable adsorption geometry, first-principles DFT can simulate the bond formation and breaking upon adsorption, which makes it more beneficial in comparison with other theoretical tools. Further, this approach exhibits similar accuracy to first principles DFT methods but does with a significant reduction in computational cost. To find the most stable adsorption geometries, three different adsorption modes are simulated by the first-principles DFT method, and their corresponding interaction energies and projected density of states (PDOS) are analyzed. Fig. 11 shows the optimized adsorption configuration of the three adsorption modes and their PDOS plots. It can be observed that adsorption configurations in Fig. 11a and b show no bonding with iron atoms. In Fig. 11a (Conf I), the HTH molecule is initially placed parallel to the top layer of Fe(1 1 0) surface so the 5-Methoxyindole part is close to the iron layer. In this configuration, distances between HTH atoms and iron atoms are within 3 Å, without forming any bond, which mostly suggests that only physical interactions can occur. The same conclusions can be made in the case of the second configuration in Fig. 11b (Conf II), where hydrazone and chlorophenyl moieties are initially placed parallel to the iron top layer. In contrast, when the HTH molecule is placed entirely parallel to the top layer of the iron surface (Conf III), it shows the formation of 4 bonds between C and O atoms with the iron surface. The formed bonds have bond distances of 2.25–2.29 and 1.97 Å for C-Fe and O-Fe, respectively. It has been reported that the sum of the covalent radii value for Fe-C ($r_C + r_{Fe}$) and Fe-O ($r_O + r_{Fe}$) are 2.08 and 1.98 Å, respectively (Cordero et al., 2008). Compared with all bond distances mentioned above, it can be said that all length distances are within the sum of covalent radii values of Fe-C and Fe-O, thus indicating the formation of covalent bonds. In terms of interactive force, the absolute values of interaction energy show the following trend: Conf III (-2.14 eV) > Conf II (-0.08 eV) > Conf I (-0.03 eV). The Conf III exhibits a significantly higher negative interaction energy value compared to other configurations. It strengthens the known fact that parallel adsorption mode is the most stable adsorption configuration of large-size organic compounds (Guo et al., 2017).

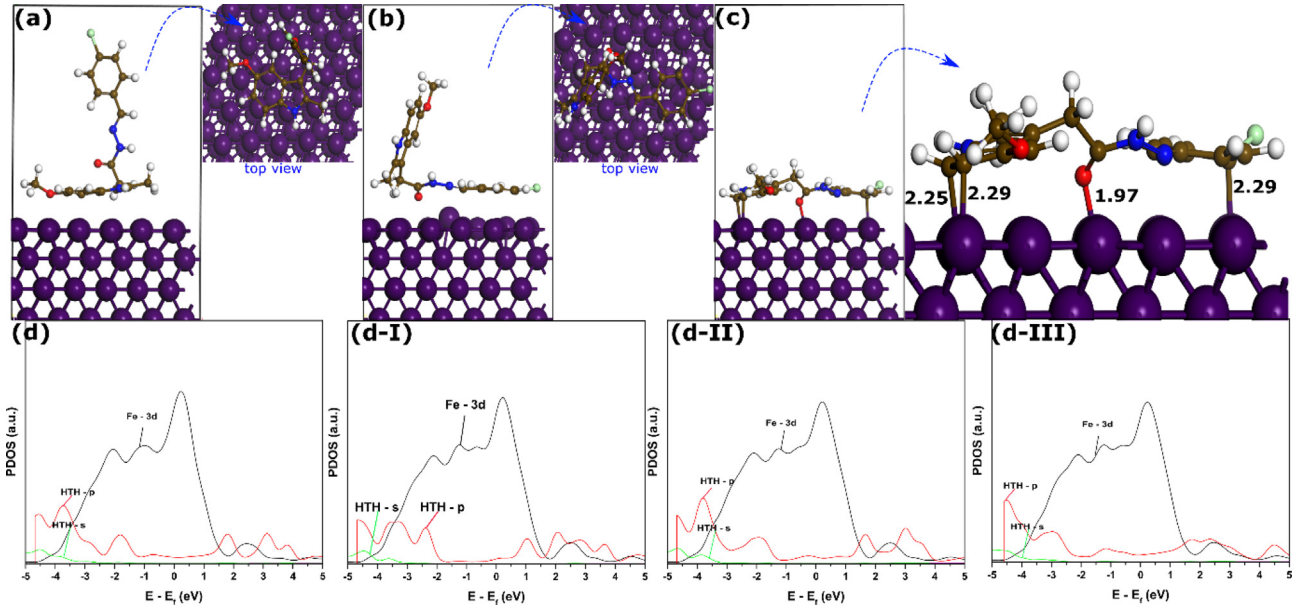

Fig. 11 The optimized adsorption geometries and projected density of states of different configurations of HTH molecule on Fe(1 1 0) surface by SCC-DFTB method; Conf I (a), Conf II (b), and Conf III (c), and PDOSs (d). Bond lengths are in Å.

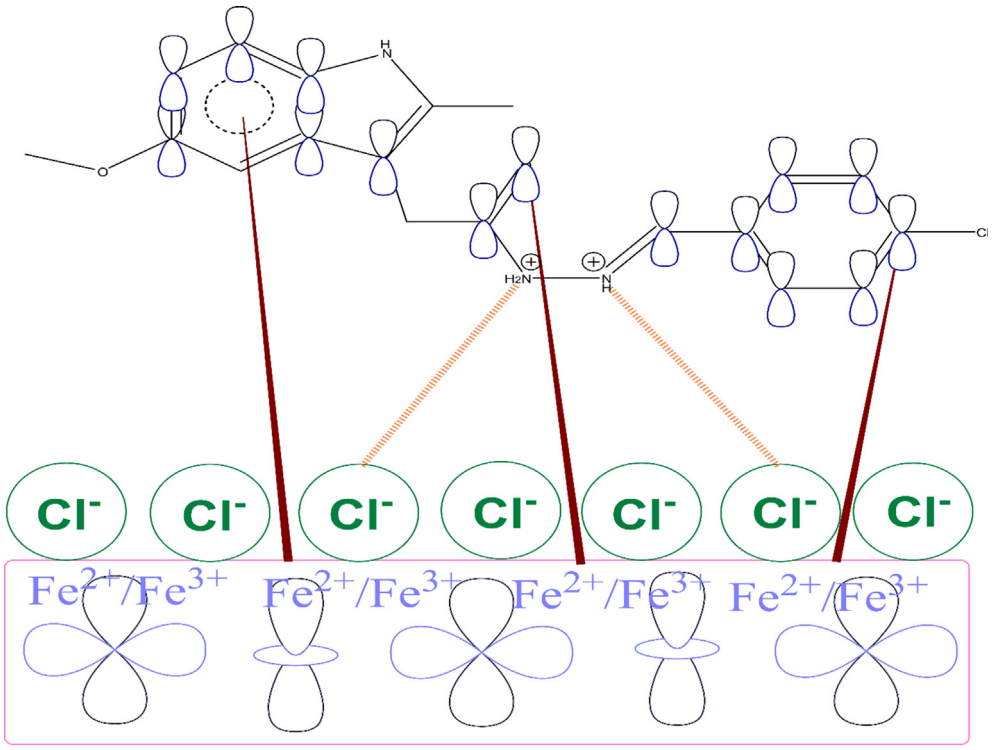

Fig. 12 A schematic representation of the adsorption of HTH on steel surface.

To get further information about the nature of binding of the inhibitor molecule with iron atoms, PDOSs are analyzed as shown in Fig. 11d-I, 11d-II, and 11d-III for Conf I, Conf II, and Conf III, respectively. Fig. 11d shows the PDOS of the HTH molecule before adsorption for comparison. By comparison, it can be seen that most of the peaks related to the chemical states of Conf I and Conf II keep relatively similar shapes and intensities to those before adsorption. However, significant changes to peaks contributed by s- and p-orbitals of Conf III are observed, which is mainly attributed to orbital mixing between molecules' orbitals, especially p-orbitals and Fe *d* orbitals. It indicates that bonds formed between HTH's molecule and iron atoms are covalent bonds (Kumar et al., 2022, 2020).

3.7. Corrosion inhibition mechanism of hydrazone

Hydrazone is one of the most effective organic classes for preventing carbon steel corrosion in acid solutions thanks to its unique structural characteristics (Khamaysa et al., 2020). However, research into the extent to which the chemical composition influences the efficiency of the hydrazone inhibitor mechanism of action on the surface of carbon steel in 1 mol/L HCl solution is still ongoing. To extend the discussion, we relied on numerous interpretations of previous studies on the mechanism of hydrazone adsorption on the surface of carbon steel (Lgaz et al., 2020a). First of all, because the metal is in a hydrochloric acid solution, it has a positive charge on its surface (Solmaz, 2014a, 2014b). The inhibitor under study is likely to be protonated in this medium. In this state, the metal's positive charge favours the adsorption of chlorides (Cl^-) on its surface (Ouakki et al., 2021), forming a bridge between the charged metallic surface and protonated inhibitor molecules (Lgaz et al., 2020a; Ouakki et al., 2021).

After quick physical attractions, hydrazone molecules are mainly chemically adsorbed on the surface of carbon steel. It is believed that the presence of electron-rich aromatic rings and heteroatoms will boost the transfer of loosely bound electrons from molecules to electron-deficient iron orbitals. The presence of two aromatic rings in the inhibitor's molecule allows it to transfer electrons to vacant iron orbitals in this process (Lgaz et al., 2020a). In view of experimental and theoretical findings, it can be concluded that the HTH molecule exhibits mixed physicochemical interactions with iron atoms. As shown from first-principles DFT simulations, HTH molecules tend to be more stable when parallelly adsorbing on the steel surface, forming several covalent bonds. The strong affinity and binding with iron atoms make the formed inhibitor layer stronger and more stable even at high temperatures. A schematic representation of the possible corrosion inhibition is shown in Fig. 12.

4. Conclusion

In the present work, electrochemical and computational studies were used to determine the effect of a hydrazone inhibitor on the corrosion of carbon steel in acid solution at temperatures ranging from 303 K to 333 K. According to the findings of the influence of concentration and temperature, the tested hydrazone can be classified as an efficient corrosion inhibitor, with an efficacy of around 94% and 89% at 303 and 333 K, respectively. These efficiencies imply that the hydrazone molecules were strongly adsorbed on the iron surface following a mixed physical and chemical adsorption. According to the polarization data, the hydrazone can be classified as a mixed-type inhibitor, significantly blocking both anodic and cathodic corrosion reactions. The polariza-

tion resistance increased, and the effective double-layer capacitance decreased significantly after adding an increasing amount of tested inhibitor. The temperature effect led to the conclusion that the effectiveness of the hydrazone was not significantly affected at temperatures ranging from 303 K to 332 K. Computational studies by DFT, MD, and first-principles DFT simulations revealed the formation of several covalent bonds when the HTH molecule is parallelly adsorbed on the iron surface. To back up the findings, and in comparison, to earlier research, the presence of several reactive sites and heteroatoms boosts the effectiveness of the hydrazone and increases the steel's corrosion resistance owing to the strong interactions through charge transfer and hybridization between HTH's p-orbitals and vacant *d*-orbitals of iron atoms.

Acknowledgments

This work was supported by Researchers Supporting Project Number (RSP2023R100), King Saud University, Riyadh, Saudi Arabia. This work was supported by the National Research Foundation of Korea (NRF) grant funded by the Korea government (MSIT) (No. NRF-2018R1A5A1025137). The authors would like to thank the Deanship of Scientific Research at Umm Al-Qura University for supporting this work by Grant Code: 22UQU4331201DSR01.

Appendix A. Supplementary material

Supplementary data to this article can be found online at https://doi.org/10.1016/j.arabjc.2023.104711.

References

Bassey, I., 2014. Recent Advances in Computational Design of Organic Materials for Corrosion Protection of Steel in Aqueous Media, in: Aliofkhazraei, M. (Ed.), Developments in Corrosion Protection. InTech. https://doi.org/10.5772/57245.

Bockris, J.O., Reddy, A.K.N., Gamboa-Aldeco, M.E., 1998. Modern Electrochemistry 2B: Electrodics in Chemistry, Engineering, Biology and Environmental Science. Springer Science & Business Media.

Chafai, N., Chafaa, S., Benbouguerra, K., Hellal, A., 2019. Synthesis, spectral analysis, anti-corrosive activity and theoretical study of an aromatic hydrazone derivative. J. Mol. Struct. 1181, 83–92. https://doi.org/10.1016/j.molstruc.2018.12.073.

Chafiq, M., Chaouiki, A., Albayati, M.R., Lgaz, H., Salghi, R., AbdelRaheem, S.K., Ali, I.H., Mohamed, S.K., Chung, I.M., 2020a. Unveiled understanding on corrosion inhibition mechanisms of hydrazone derivatives based on naproxen for mild steel in HCl: a joint experimental/theoretical study. J. Mol. Liq. 320,. https://doi.org/10.1016/j.molliq.2020.114442 114442.

Chafiq, M., Chaouiki, A., Lgaz, H., Salghi, R., Gaonkar, S.L., Bhat, K.S., Marzouki, R., Ali, I.H., Khan, M.I., Shimizu, H., Chung, I. M., 2020b. Synthesis and corrosion inhibition evaluation of a new schiff base hydrazone for mild steel corrosion in HCl medium: electrochemical, DFT, and molecular dynamics simulations studies. J. Adhes. Sci. Technol. 34, 1283–1314. https://doi.org/10.1080/01694243.2019.1707561.

Chafiq, M., Chaouiki, A., Al-Hadeethi, M.R., Salghi, R., Ismat, H., Shaaban, K., Chung, I.-M., 2021. A joint experimental and theoretical investigation of the corrosion inhibition behavior and mechanism of hydrazone derivatives for mild steel in HCl solution. Colloids Surf. A Physicochem. Eng. Asp 610,. https://doi.org/10.1016/j.colsurfa.2020.125744 125744.

Chaitra, T.K., Mohana, K.N., Gurudatt, D.M., Tandon, H.C., 2016. Inhibition activity of new thiazole hydrazones towards mild steel corrosion in acid media by thermodynamic, electrochemical and quantum chemical methods. J. Taiwan Inst. Chem. Eng. 67, 521–531. https://doi.org/10.1016/j.jtice.2016.08.013.

Chaouiki, A., Chafiq, M., Al-Hadeethi, M.R., Lgaz, H., Salghi, R., Abdelraheem, S.K., Ali, I.H., Ebraheem, S.A.M., Chung, I.M., Mohamed, S.K., 2020a. Exploring the corrosion inhibition effect of two hydrazone derivatives for mild steel corrosion in 1.0 M HCl solution via electrochemical and surface characterization studies. Int. J. Electrochem. Sci. 15, 9354–9377. https://doi.org/10.20964/2020.09.95.

Chaouiki, A., Chafiq, M., Lgaz, H., Al-Hadeethi, M.R., Ali, I.H., Masroor, S., Chung, I.-M., 2020b. Green Corrosion Inhibition of Mild Steel by Hydrazone Derivatives in 1.0 M HCl. Coatings 10, 640. https://doi.org/10.3390/coatings10070640.

Chkirate, K., Azgaou, K., Elmsellem, H., El Ibrahimi, B., Sebbar, N. K., Anouar, E.H., Benmessaoud, M., El Hajjaji, S., Essassi, E.M., 2021. Corrosion inhibition potential of 2-[(5-methylpyrazol-3-yl) methyl]benzimidazole against carbon steel corrosion in 1 M HCl solution: combining experimental and theoretical studies. J. Mol. Liq. 321,. https://doi.org/10.1016/j.molliq.2020.114750 114750.

Cordero, B., Gómez, V., Platero-Prats, E., Revés, M., Echeverría, J., Cremades, E., Barragán, F., Alvarez, S., 2008. Covalent radii revisited. Dalton Trans., 2832–2838 https://doi.org/10.1039/B801115J.

Damej, M., Skal, S., Aslam, J., Zouarhi, M., Erramli, H., Alrashdi, A. A., Lee, H., El, Y., Lgaz, H., 2022. An environmentally friendly formulation based on Cannabis Sativa L. seed oil for corrosion inhibition of E24 steel in HCl medium: experimental and theoretical study. Colloids Surf. A Physicochem. Eng. Asp 643,. https://doi.org/10.1016/j.colsurfa.2022.128745 128745.

Damej, M., Molhi, A., Lgaz, H., Hsissou, R., Aslam, J., Benmessaoud, M., Rezki, N., Lee, H.-S., Lee, D.-E., 2023. Performance and interaction mechanism of a new highly efficient benzimidazole-based epoxy resin for corrosion inhibition of carbon steel in HCl: a study based on experimental and first-principles DFTB simulations. J. Mol. Struct. 1273,. https://doi.org/10.1016/j.molstruc.2022.134232 134232.

Dehghani, A., Bahlakeh, G., Ramezanzadeh, B., Ramezanzadeh, M., 2019. A combined experimental and theoretical study of green corrosion inhibition of mild steel in HCl solution by aqueous Citrullus lanatus fruit (CLF) extract. J. Mol. Liq. 279, 603–624. https://doi.org/10.1016/j.molliq.2019.02.010.

Dehri, I., Özcan, M., 2006. The effect of temperature on the corrosion of mild steel in acidic media in the presence of some sulphur-containing organic compounds. Mater. Chem. Phys. 98, 316–323. https://doi.org/10.1016/j.matchemphys.2005.09.020.

Döner, A., Solmaz, R., Özcan, M., Kardaş, G., 2011. Experimental and theoretical studies of thiazoles as corrosion inhibitors for mild steel in sulphuric acid solution. Corros. Sci. 53, 2902–2913. https://doi.org/10.1016/j.corsci.2011.05.027.

Dutta, A., Saha, S.K., Banerjee, P., Sukul, D., 2015. Correlating electronic structure with corrosion inhibition potentiality of some bis-benzimidazole derivatives for mild steel in hydrochloric acid: Combined experimental and theoretical studies. Corros. Sci. 98, 541–550. https://doi.org/10.1016/j.corsci.2015.05.065.

Dutta, A., Saha, S.K., Adhikari, U., Banerjee, P., Sukul, D., 2017. Effect of substitution on corrosion inhibition properties of 2-(substituted phenyl) benzimidazole derivatives on mild steel in 1M HCl solution: a combined experimental and theoretical approach. Corros. Sci. 123, 256–266. https://doi.org/10.1016/j.corsci.2017.04.017.

Ebenso, E.E., Verma, C., Olasunkanmi, L.O., Akpan, E.D., Verma, D. K., Lgaz, H., Guo, L., Kaya, S., Quraishi, M.A., 2021. Molecular modelling of compounds used for corrosion inhibition studies: a review. Phys. Chem. Chem. Phys. 23, 19987–20027. https://doi.org/10.1039/D1CP00244A.

Fadhil, A.A., Khadom, A.A., Liu, H., Fu, C., Wang, J., Fadhil, N.A., Mahood, H.B., 2019. (S)-6-Phenyl-2,3,5,6-tetrahydroimidazo[2,1-

b] thiazole hydrochloride as corrosion inhibitor of steel in acidic solution: Gravimetrical, electrochemical, surface morphology and theoretical simulation. J. Mol. Liq. 276, 503–518. https://doi.org/10.1016/j.molliq.2018.12.015.

Gece, G., 2008. The use of quantum chemical methods in corrosion inhibitor studies. Corros. Sci. 50, 2981–2992. https://doi.org/10.1016/j.corsci.2008.08.043.

Gómez, B., Likhanova, N.V., Domínguez-Aguilar, M.A., Martínez-Palou, R., Vela, A., Gázquez, J.L., 2006. Quantum Chemical Study of the Inhibitive Properties of 2-Pyridyl-Azoles. J. Phys. Chem. B 110, 8928–8934. https://doi.org/10.1021/jp057143y.

Grimme, S., 2006. Semiempirical GGA-type density functional constructed with a long-range dispersion correction. J. Comput. Chem. 27, 1787–1799.

Guo, L., Qi, C., Zheng, X., Zhang, R., Shen, X., Kaya, S., 2017. Toward understanding the adsorption mechanism of large size organic corrosion inhibitors on an Fe(110) surface using the DFTB method. RSC Adv. 7, 29042–29050. https://doi.org/10.1039/C7RA04120A.

Guo, L., Tan, J., Kaya, S., Leng, S., Li, Q., Zhang, F., 2020. Multidimensional insights into the corrosion inhibition of 3,3-dithiodipropionic acid on Q235 steel in H_2SO_4 medium: a combined experimental and in silico investigation. J. Colloid Interface Sci. 570, 116–124. https://doi.org/10.1016/j.jcis.2020.03.001.

Han, Y., Liu, W., Chen, J., 2016. DFT simulation of the adsorption of sodium silicate species on kaolinite surfaces. Appl. Surf. Sci. 370, 403–409. https://doi.org/10.1016/j.apsusc.2016.02.179.

Heidari, Z., Pelalak, R., Malekshah, R.E., Pishnamazi, M., Marjani, A., Sarkar, S.M., Shirazian, S., 2021. Molecular modeling investigation on mechanism of cationic dyes removal from aqueous solutions by mesoporous materials. J. Mol. Liq. 329,. https://doi.org/10.1016/j.molliq.2021.115485 115485.

Id, O., Mouden, E.L., Batah, A., Belkhaouda, M., Salghi, R., Chetouani, A., 2021. Inhibition of Mild Steel Corrosion in 1M Hydrochloric Medium by the cherimoya seeds 3, 588–601.

Islam, N., Kaya, S., 2018. Conceptual Density Functional Theory and Its Application in the Chemical Domain. CRC Press.

Khamaysa, O.M.A., Selatnia, I., Zeghache, H., Lgaz, H., Sid, A., Chung, I.M., Benahmed, M., Gherraf, N., Mosset, P., 2020. Enhanced corrosion inhibition of carbon steel in HCl solution by a newly synthesized hydrazone derivative: Mechanism exploration from electrochemical, XPS, and computational studies. J. Mol. Liq. 315,. https://doi.org/10.1016/j.molliq.2020.113805 113805.

Khamaysa, O.M.A., Selatnia, I., Lgaz, H., Sid, A., Lee, H.-S., Zeghache, H., Benahmed, M., Ali, I.H., Mosset, P., 2021. Hydrazone-based green corrosion inhibitors for API grade carbon steel in HCl: Insights from electrochemical, XPS, and computational studies. Colloids Surf. A Physicochem. Eng. Asp 626. https://doi.org/10.1016/j.colsurfa.2021.127047.

Kokalj, A., 2021. Molecular modeling of organic corrosion inhibitors: Calculations, pitfalls, and conceptualization of molecule–surface bonding. Corros. Sci. 193. https://doi.org/10.1016/j.corsci.2021.109650.

Kokalj, A., 2022. Corrosion inhibitors: physisorbed or chemisorbed? Corros. Sci. 196,. https://doi.org/10.1016/j.corsci.2021.109939 109939.

Kokalj, A., Lozinšek, M., Kapun, B., Taheri, P., Neupane, S., Losada-Pérez, P., Xie, C., Stavber, S., Crespo, D., Renner, F.U., Mol, A., Milošev, I., 2021. Simplistic correlations between molecular electronic properties and inhibition efficiencies: Do they really exist? Corros. Sci. 179,. https://doi.org/10.1016/j.corsci.2020.108856 108856.

Kumar, D., Jain, V., Rai, B., 2020. Imidazole derivatives as corrosion inhibitors for copper: A DFT and reactive force field study. Corros. Sci. 171,. https://doi.org/10.1016/j.corsci.2020.108724 108724.

Kumar, D., Jain, V., Rai, B., 2022. Capturing the synergistic effects between corrosion inhibitor molecules using density functional theory and ReaxFF simulations - A case for benzyl azide and butyn-1-ol on Cu surface. Corros. Sci. 195,. https://doi.org/10.1016/j.corsci.2021.109960 109960.

Lgaz, H., Chaouiki, A., Albayati, M.R., Salghi, R., El Aoufir, Y., Ali, I.H., Khan, M.I., Mohamed, S.K., Chung, I.M., 2019. Synthesis and evaluation of some new hydrazones as corrosion inhibitors for mild steel in acidic media. Res. Chem. Intermed. 45, 2269–2286. https://doi.org/10.1007/s11164-018-03730-y.

Lgaz, H., Chung, I.M., Albayati, M.R., Chaouiki, A., Salghi, R., Mohamed, S.K., 2020a. Improved corrosion resistance of mild steel in acidic solution by hydrazone derivatives: an experimental and computational study. Arab. J. Chem. 13, 2934–2954. https://doi.org/10.1016/j.arabjc.2018.08.004.

Lgaz, H., Chaouiki, A., Lamouri, R., Salghi, R., Lee, H.-S., 2021. Computational Methods of Corrosion Inhibition Assessment, in: Sustainable Corrosion Inhibitors I: Fundamentals, Methodologies, and Industrial Applications, ACS Symposium Ser. Am. Chem. Soc., pp. 87–109. https://doi.org/10.1021/bk-2021-1403.ch006.

Lgaz, H., Lee, H., 2022. Facile preparation of new hydrazone compounds and their application for long-term corrosion inhibition of N80 steel in 15% HCl: an experimental study combined with DFTB calculations. J. Mol. Liq. 347,. https://doi.org/10.1016/j.molliq.2021.117952 117952.

Lgaz, H., Salghi, R., Masroor, S., Kim, S.H., Kwon, C., Kim, S.Y., Yang, Y.J., Chung, I.M., 2020b. Assessing corrosion inhibition characteristics of hydrazone derivatives on mild steel in HCl: Insights from electronic-scale DFT and atomic-scale molecular dynamics. J. Mol. Liq. 308,. https://doi.org/10.1016/j.molliq.2020.112998 112998.

Mehmeti, V., Podvorica, F.I., 2018. Experimental and Theoretical Studies on Corrosion Inhibition of Niobium and Tantalum Surfaces by Carboxylated Graphene Oxide. Materials 11, 893. https://doi.org/10.3390/ma11060893.

Mohamed, S.K., Mague, J.T., Akkurt, M., Mohamed, A.F., Albayati, M.R., 2015. Crystal structure of 2-(2, 3-dimethylanilino)-N′-[(1E)-2-hydroxybenzylidene] benzohydrazide. Acta Crystallographica Section E: Crystallographic Commun. 71, o957–o958.

Nwokolo, I.K., Shi, H., Ikeuba, A.I., Gao, N., Li, J., Ahmed, S., Liu, F., 2022. ZnMOF-BTA , on Carbon Steel in HCl Solution.

Obot, I.B., Macdonald, D.D., Gasem, Z.M., 2015. Density functional theory (DFT) as a powerful tool for designing new organic corrosion inhibitors. Part 1: an overview. Corros. Sci. 99, 1–30. https://doi.org/10.1016/j.corsci.2015.01.037.

Obot, I.B., Haruna, K., Saleh, T.A., 2018. Atomistic simulation: a unique and powerful computational tool for corrosion inhibition research. Arab J. Sci. Eng. https://doi.org/10.1007/s13369-018-3605-4.

Olasunkanmi, L.O., Kabanda, M.M., Ebenso, E.E., 2016. Quinoxaline derivatives as corrosion inhibitors for mild steel in hydrochloric acid medium: electrochemical and quantum chemical studies. Physica E 76, 109–126. https://doi.org/10.1016/j.physe.2015.10.005.

Ouakki, M., Galai, M., Benzekri, Z., Verma, C., Ech-chihbi, E., Kaya, S., Boukhris, S., Ebenso, E.E., Touhami, M.E., Cherkaoui, M., 2021. Insights into corrosion inhibition mechanism of mild steel in 1 M HCl solution by quinoxaline derivatives: electrochemical, SEM/EDAX, UV-visible, FT-IR and theoretical approaches. Colloids Surf. A: Physicochem. Eng. Aspects Elsevier B.V. https://doi.org/10.1016/j.colsurfa.2020.125810.

Oyekunle, D.T., Agboola, O., Ayeni, A.O., 2019. Corrosion inhibitors as building evidence for mild steel: a review. J. Phys. Conf. Ser. 1378. https://doi.org/10.1088/1742-6596/1378/3/032046.

Pareek, S., Jain, D., Hussain, S., Biswas, A., Shrivastava, R., Parida, S. K., Kisan, H.K., Lgaz, H., Chung, I.-M., Behera, D., 2019. A new insight into corrosion inhibition mechanism of copper in aerated 3.5 wt.% NaCl solution by eco-friendly Imidazopyrimidine Dye: experimental and theoretical approach. Chem. Eng. J. 358, 725–742. https://doi.org/10.1016/j.cej.2018.08.079.

Perdew, J.P., Burke, K., Ernzerhof, M., 1996. Generalized gradient approximation made simple. Phys. Rev. Lett. 77, 3865.

Quadri, T.W., Olasunkanmi, L.O., Fayemi, O.E., Lgaz, H., Dagdag, O., Sherif, E.-S.-M., Alrashdi, A.A., Akpan, E.D., Lee, H.-S., Ebenso, E.E., 2022. Computational insights into quinoxaline-based corrosion inhibitors of steel in HCl: Quantum chemical analysis and QSPR-ANN studies. Arab. J. Chem. 15, 103870.

Riasová, P., Doubková, D., Pincová, L., Jung, O., Polášek, M., Jáč, P., 2018. Development of micellar electrokinetic chromatography method for the determination of three defined impurities in indomethacin. Electrophoresis 39, 2550–2557.

Saha, S.K., Murmu, M., Murmu, N.C., Banerjee, P., 2016. Evaluating electronic structure of quinazolinone and pyrimidinone molecules for its corrosion inhibition effectiveness on target specific mild steel in the acidic medium: a combined DFT and MD simulation study. J. Mol. Liq. 224, 629–638. https://doi.org/10.1016/j.molliq.2016.09.110.

Salghi, R., Jodeh, S., Ebenso, E.E., Lgaz, H., Ben Hmamou, D., Belkhaouda, M., Ali, I.H., Messali, M., Hammouti, B., Fattouch, S., 2017. Inhibition of C-steel corrosion by green tea extract in hydrochloric solution. Int. J. Electrochem. Sci. 12, 3283–3295. https://doi.org/10.20964/2017.04.46.

Serhan, M., Sprowls, M., Jackemeyer, D., Long, M., Perez, I.D., Maret, W., Tao, N., Forzani, E., 2019. Total iron measurement in human serum with a smartphone. In: AIChE Annual Meeting, Conference Proceedings 2019-Novem. https://doi.org/10.1039/x0xx00000x.

Shahmoradi, A.R., Talebibahmanbigloo, N., Nickhil, C., Nisha, R., Javidparvar, A.A., Ghahremani, P., Bahlakeh, G., Ramezanzadeh, B., 2022. Molecular-MD/atomic-DFT theoretical and experimental studies on the quince seed extract corrosion inhibition performance on the acidic-solution attack of mild-steel. J. Mol. Liq. 346,. https://doi.org/10.1016/j.molliq.2021.117921 117921.

Shanbhag, A.V., Venkatesha, T.V., Prabhu, R.A., Kalkhambkar, R. G., Kulkarni, G.M., 2008. Corrosion inhibition of mild steel in acidic medium using hydrazide derivatives. J. Appl. Electrochem. 38, 279–287. https://doi.org/10.1007/s10800-007-9436-8.

Singh, D.K., Kumar, S., Udayabhanu, G., John, R.P., 2016. 4(N, N-dimethylamino) benzaldehyde nicotinic hydrazone as corrosion inhibitor for mild steel in 1 M HCl solution: An experimental and theoretical study. J. Mol. Liq. 216, 738–746. https://doi.org/10.1016/j.molliq.2016.02.012.

Singh, A.K., Singh, P., 2015. Adsorption behaviour of o-hydroxy acetophenone benzoyl hydrazone on mild steel/hydrochloric acid interface. J. Ind. Eng. Chem. 21, 552–560. https://doi.org/10.1016/j.jiec.2014.03.018.

Singh, A.K., Thakur, S., Pani, B., Chugh, B., Lgaz, H., Chung, I.-M., Chaubey, P., Pandey, A.K., Singh, J., 2019. Solvent-free microwave assisted synthesis and corrosion inhibition study of a series of hydrazones derived from thiophene derivatives: experimental, surface and theoretical study. J. Mol. Liq. 283, 788–803. https://doi.org/10.1016/j.molliq.2019.03.126.

Solmaz, R., 2014a. Investigation of adsorption and corrosion inhibition of mild steel in hydrochloric acid solution by 5-(4-Dimethylaminobenzylidene)rhodanine. Corros. Sci. 79, 169–176. https://doi.org/10.1016/j.corsci.2013.11.001.

Solmaz, R., 2014b. Investigation of corrosion inhibition mechanism and stability of Vitamin B1 on mild steel in 0.5M HCl solution. Corros. Sci. 81, 75–84. https://doi.org/10.1016/j.corsci.2013.12.006.

Tammara, V.K., Narurkar, M.M., Crider, A.M., Khan, M.A., 1994. Morpholinoalkyl ester prodrugs of diclofenac: synthesis, in vitro and in vivo evaluation. J. Pharm. Sci. 83, 644–648.

Tang, J., Hu, Y., Han, Z., Wang, H., Zhu, Y., Wang, Y., Nie, Z., Wang, Y., 2018. Experimental and Theoretical Study on the Synergistic Inhibition Effect of Pyridine Derivatives and Sulfur-Containing Compounds on the Corrosion of Carbon Steel in CO2-Saturated 3.5 wt.% NaCl Solution. Molecules 23, 3270. https://doi.org/10.3390/molecules23123270.

Vargas, D.F., Romero, B.S., Kaufman, T.S., Larghi, E.L., 2021. On the Use of $CeCl_{3.7}H_2O$ as a catalyst for the synthesis of hydrazones derived from aromatic aldehydes and ketones 82. https://doi.org/10.3390/ecsoc-24-08095.

Verma, C., Olasunkanmi, L.O., Ebenso, E.E., Quraishi, M.A., 2018. Substituents effect on corrosion inhibition performance of organic compounds in aggressive ionic solutions: a review. J. Mol. Liq. 251, 100–118. https://doi.org/10.1016/j.molliq.2017.12.055.

Walczak, M.S., Morales-Gil, P., Lindsay, R., 2019. Determining Gibbs energies of adsorption from corrosion inhibition efficiencies: is it a reliable approach? Corros. Sci. 155, 182–185. https://doi.org/10.1016/j.corsci.2019.04.040.

Weston, M., Reade, T.J., Handrup, K., Champness, N.R., O'Shea, J. N., 2012. Adsorption of dipyrrin-based dye complexes on a rutile TiO_2 (110) Surface. J. Phys. Chem. C 116, 18184–18192. https://doi.org/10.1021/jp3025864.

Zaher, A., Aslam, R., Lee, H.-S., Khafouri, A., Boufellous, M., Alrashdi, A.A., El Aoufir, Y., Lgaz, H., Ouhssine, M., 2022. A combined computational & electrochemical exploration of the Ammi visnaga L. extract as a green corrosion inhibitor for carbon steel in HCl solution. Arab. J. Chem. 15,. https://doi.org/10.1016/j.arabjc.2021.103573 103573.